STOCHASTIC EXCITATION OF THE SOLAR OSCILLATIONS BY TURBULENT CONVECTION

Thesis by
Gregory Thomas Willette

In Partial Fulfillment of the Requirements
for the Degree of
Doctor of Philosophy

California Institute of Technology
Pasadena, California

1994
(Submitted May 23, 1994)

ACKNOWLEDGEMENTS

To order of magnitude, this thesis may not have been possible without the generous assistance and encouragement of my advisor, Prof. Peter Goldreich. In addition, my mentor and collaborator of many years, Dr. Stirling Colgate, has contributed significantly to my growth as a scientist.

During my time at the Institute, I have benefited greatly from discussions with TAPIR postdocs Dr. Norm Murray, Dr. Sridhar Seshadri, Dr. Robert Emering, and Dr. Melvyn Davies, as well as fellow graduate students Yanqin Wu, Alice Quillen and Andreas Reisenegger. The lecture courses by Prof. Joel Franklin, Prof. Gerald Whitham, Prof. Noel Corngold, Prof. Bill Johnson, and Prof. Roy Gould rank as true highpoints of my Caltech experience.

The observations presented in this thesis were facilitated by the expert help of the BBSO staff: Dr. Alan Patterson, Bill Marquette, Randy Fear, Dr. John Varsik, and Glenn Eychaner. Prof. Hal Zirin was a source of inspiration and practical wisdom during my observation runs at Big Bear. Scientific consultations with Prof. Ken Libbrecht, Dr. Martin Woodard, Dr. Haimin Wang, and Dr. James Kaufman were always appreciated.

This work was supported by NSF and NASA grants, by a Graduate Research Assistantship at Los Alamos National Laboratory, by a Graduate Fellowship from the Office of Naval Research, and by Teaching Assistantships in Physics and Applied Mathematics.

To Bud and Kay

ABSTRACT

The thesis topic is the stochastic excitation of the solar p-modes by turbulent convection, and the work consists of four parts: three theoretical sections and one observational. In the first section of the thesis, an explicit calculation of the acoustic radiation of a buoyant oscillating bubble is presented as a model for the excitation of the solar p-modes. The central scientific issue addressed in this work is the cancellation of monopole and dipole radiation fields in an anisotropic medium, first pointed out by Goldreich and Kumar (1990). When the bubble oscillation frequency is small compared to the acoustic cutoff, the monopole and dipole disturbances cancel to the quadrupole order in the far field. The second section deals with the role of convective structures in a wide number of problems, including the creation of acoustic disturbances, the transport of heat and magnetic fields, and the penetration of flows into stable layers of the atmosphere (overshoot). A model of plume convection is developed to discuss these issues. It is argued that the scaleheight-sized flows (the only energetically significant ones) are properly characterized as coherent, entropy-preserving plumes, in contradistinction to the picture of amorphous parcels of fluid suggested by the Mixing Length Theory, and in spite of the large Reynolds numbers typical in astrophysical convection. The third section of the thesis is an analysis of high-resolution surface velocity data taken with a magneto-optical filter on the 10 inch telescope at Big Bear Solar Observatory. Estimates are obtained for the frequencies and amplitudes of the solar oscillations of high spherical harmonic degree ($l \lesssim 2000$). The observed mode energies follow a Boltzmann distribution ($P(E) \propto \exp\{-E/\overline{E}\}$), as is predicted in the stochastic excitation model. In the final section of the thesis, a derivation of the variational principle for an incompressible fluid is presented. The Lagrange and Hamiltonian densities are calculated to third order in the displacement field, and these results are suitable to study the non-linear interactions among incompressible modes.

TABLE OF CONTENTS

COPYRIGHT ii

ACKNOWLEDGEMENTS iii

DEDICATION iv

ABSTRACT v

TABLE OF CONTENTS vi

CHAPTER 1 Introduction 1

1.1 Historical Context 1

1.2 Overview of Thesis 4

Chapter 1 References 7

CHAPTER 2 Acoustic Radiation of a Buoyant Sphere 9

2.1 Introduction 9

2.2 Statement of the Problem 11

2.3 The Polytropic Acoustic Green's Function 14

2.4 Lowest Order Solutions 21

2.5 Discussion 25

Appendix 2.1 27

Appendix 2.2 30

Appendix 2.3 31

Appendix 2.4 33

Appendix 2.5 36

Chapter 2 References 42

CHAPTER 3 A Simple Model of Plume Convection 43

3.1 Introduction 44

3.2 The Plume Model 47

3.3 Implications of the Model 53

3.4 Discussion 62

Appendix 3.1 64

Appendix 3.2 66

Chapter 3 References 67

CHAPTER 4 Observations of High Degree Solar p-Modes . . 68

4.1 Introduction 68

4.2 Description of Data Set 70

4.3 Data Reduction and Analysis 72

4.4 Discussion 79

Appendix 4.1 80

Chapter 4 References 84

CHAPTER 5 Variational Principle for an Incompressible Fluid 85

5.1 Introduction 85

5.2 Derivation of the Principle 86

5.3 Discussion 94

Appendix 5.1 95

Appendix 5.2 97

Chapter 5 References 98

CHAPTER 1

Introduction

A brief review of helioseismology is presented, followed by a broad overview of the thesis results. Emphasis is placed on the background relevant to our work.

1.1 Historical Context

Solar oscillations with a 5 minute period were discovered in the early 1960s by Leighton *et al.* (Leighton, Noyes and Simon (1962); Evans and Michard (1963)).† These observed 'wave packets' were originally interpreted as *local* disturbances, traveling along the surface, and possibly launched by strong turbulent motions in the upper convection zone (below the photosphere). This characterization remains plausible since the wave period matches the eddy turnover time for subphotospheric convective cells.

† The basic technique for observing these oscillations makes use of the Doppler effect: absorption lines formed in a moving layer near the photosphere are shifted in frequency, and an approximate linear relationship exists between the frequency shift and line-of-sight velocity. A spatially resolved measurement of this type is called a Dopplergram, or velocity image. Photospheric oscillations can also be seen in brightness fluctutations, since the emitting material travels through regions of different opacity. The latter effect is more difficult to quantify, however, because the correspondence between signal and velocity depends sensitively on the radiative transfer model.

Nearly a decade passed before Ulrich (1970) and Leibacher and Stein (1971) argued that these oscillations are *global* sound waves resonating inside the sun. Observed photospheric motions were explained as a surface manifestation of disturbances trapped in the interior. Gradients in the sound speed (temperature) cause traveling waves to refract away from the core by Snell's Law, and internal reflection occurs at the surface due to the rise in acoustic cutoff frequency. On this basis, the normal modes of the sun can be calculated by expansion in spherical harmonics, just as one computes the energy eigenstates of the hydrogen atom in quantum mechanics. This field is known as helioseismology, and it bears considerable resemblance to its terrestrial relative.

Since the restoring force for sound waves is pressure, the eigenmodes have become known as p-modes. The dispersion relation for the p-modes (computed by Ulrich (1970) and Ando and Osaki (1975)) admits a family of acoustic branches (known as 'ridges'), each corresponding to a radial node number, n.† These ridges were subsequently seen in the high-resolution spectra of Deubner (1975). Full-disk observations then confirmed global character of the oscillations (Claverie, Isaak, McLeod, van der Raay, and Roca Cortés (1979); Grec, Fossat, and Pomerantz (1980)). These low-order observations yielded individual mode velocity amplitudes of order 20 cm/sec at the solar surface. It has been estimated that over 10^6 p-modes are excited to observable amplitudes (Libbrecht and Woodard (1991)). The modes constructively interfere to give surface motions on the order of 1 km/sec, comparable to the solar rotation and relative motion of the Earth.

Over the last three decades, the field of helioseismology has contributed much to our understanding of solar structure. Libbrecht (1988) has measured low and intermediate degree p-mode frequencies ($\ell \lesssim 150$) with an impressive

† The so-called f-modes have a special place among the solar oscillations. These are actually nodeless ($n = 0$) surface gravity waves.

accuracy of order 10^{-5}. Such data can be used to probe the interior of the sun and refine solar models. In particular, the interior rotation and temperature profiles have been determined by inspection of the splitting of frequencies in azimuthal order m. The modes of high degree are particularly important to investigate, since their eigenfunctions are localized near the surface where the acoustic radiation is thought to interact with convective eddies. Further study of this region of k-space may shed light on some long-standing problems in convection and compressible turbulence.

Much of the work in this thesis adds to the stochastic theory of p-mode excitation (Goldreich and Keeley (1977); Goldreich and Kumar (1990); Goldreich, Murray and Kumar (1994)). The theory holds that turbulent motions in the upper convection zone create acoustic disturbances which travel throughout the sun. In related work, the damping (Goldreich and Kumar (1991)), scattering (Goldreich and Murray (1994)), non-linear interactions (Kumar and Goldreich (1989)) of the p-modes with convection have also been investigated.

The stochastic excitation model orginated with a suggestion by Biermann (1946, 1947) that subphotospheric turbulence might generate acoustic waves which propagate into and heat the solar chromosphere. The formalism for studying sound generation by turbulence was supplied by Lighthill (1952, 1954) and Proudman (1952), and has become known as the Lighthill-Proudman Theory. Assuming the Kolmogov spectrum, Proudman (1952) showed that the acoustic emissivity has magnitude $\epsilon \sim \epsilon_0 M^5$, where ϵ_0 is the turbulent eddy dissipation and M is the Mach number. Stein (1967) and later Goldreich and Kumar (1988) modified this work to include the effects of density stratification. Musielak *et al.* (1994) have recently reconsidered this work in light of new models for the turbulent energy spectrum, and the theory still commands considerable attention in the literature.

Convection plays an important role in the excitation, damping and scattering of the solar oscillations. Excitation models typically make use of the

Mixing Length Theory (MLT) of Schmidt (1941), Taylor (1945) and Prandtl (1952). MLT provides adequate estimates of the convective flux and eddy velocities, but numerical simulations are causing a re-evaluation of its simplifying assumptions. (See Spruit, Nordland, and Title (1990) for a review.) It has become apparent that the structure and topology of convective flows may have implications for the modeling of sound generation events, the next step in the development of the stochastic excitation theory. Moreover, high-resolution mapping of the upper convective envelope may eventually force developments in the theory of stellar convection.

Scientific papers in helioseismology appear with frequency of order 10 μHz. For that reason, no exposition can offer complete coverage of such a popular and important field. For further information on helioseismology, the reader may wish to consult any of the numerous reviews which have appeared in the last three decades (Stein and Leibacher (1974); Deubner and Gough (1984); Christensen-Dalsgaard, Duvall, Gough, Harvey, and Rhodes (1985); Brown, Mihalas, and Rhodes (1986); Christensen-Dalsgaard (1988); Libbrecht (1988); Shibahashi (1990); Libbrecht and Woodard (1991)). The theses of Kumar (1988), Kaufman (1991) and Fernandes (1992) also give more detailed summaries of the major developments. For an overview of our current understanding of the sun at the introductory level, refer to Zirin (1988) or Stix (1989).

1.2 Overview of Thesis

The thesis contains results of both an applied and fundamental nature in the fields of helioseismology, solar and stellar structure, and astrophysical fluid dynamics. Although the various issues addressed in this work are related, any section can be considered apart from the others. Certain results are presented in Appendices intended for elaboration of points made in the main text.

In Chapter 2, the acoustic Green's function for a plane-parallel polytrope (a model for the solar convective envelope) is computed and used to calculate the excited amplitudes of the $p-$ and f-modes. The convective element

is modeled as a bubble expanding and contracting as it bobs up and down in the atmosphere. Changes in fluid volume generate monopole radiation, while the resulting buoyancy oscillation creates a dipole field. The central result of these calculations is the demonstration that the monopole and dipole radiation cancels in the far field to quadrupole order, an effect which was noted by Goldreich and Kumar (1990). This cancellation limits the p-mode amplitudes, while it is found that the f-mode cannot be excited by the combined monopole and dipole mechanisms due to its near incompressibility. The technical developments from this work may be useful for similar problems, since the polytropic approximation appropriately describes many atmospheres. For example, the Green's function can be used to calculate the evolution of sound waves launched by the expected cometary impact with Jupiter in July 1994.

The third Chapter addresses the role of structures in turbulent convection. A simple model of axisymmetric convective plumes is presented to provide a context for interpreting numerical simulations of deep compressible convection. The Morton, Taylor and Turner (1956) model of plumes is modified to study flows with a horizontal scale of order the density scaleheight in a gravitationally stratified atmosphere. The entrainment of mass and lower entropy material, which is important for plumes arising from a small source, may be neglected to an adequate approximation for the larger plumes. The braking of the flow is due to a pressure perturbation which is usually ignored in models of plumes. It is found that simultaneous conservation of mass, energy, momentum and entropy leads to a mathematical singularity in the model equations. This singularity forces the flow to diverge at some specific depth in the atmosphere which may be interpreted as a 'mixing length,' and this penetration scale is not very sensitive to the conditions at the source boundary. In addition, the model suggests a striking asymmetry between upward and downward directed plumes, as is commonly noted in numerical simulations of turbulent compressible convection (Stein and Nordlund (1989)). This work was done in collaboration with Dr. Stirling Colgate of Los Alamos National Laboratory.

Chapter 4 presents observations of high-degree solar oscillations made at Big Bear Solar Observatory with a Potassium Cacciani Cell. This work was originally motivated to reproduce the results presented in a thesis by Kaufman (1991). The data set consists of a time series of high-resolution Doppler images obtained at the center of the solar disk. The 'ridge' structure of the dispersion relation is seen clearly in the data up to the highest observed wavenumbers, and the mode amplitudes agree with the theory of Goldreich *et al.* (1994) (in order of magnitude and qualitative behavior). Moreover, the probability distribution of mode energies determined from this observation is shown to conform to a Boltzmann form, as predicted by the stochastic excitation model (see Kumar, Franklin and Goldreich (1988)).

Finally, Chapter 5 discusses variational principles for an inviscid, incompressible fluid. As a preliminary to solving problems in non-linear mode coupling, the Lagrangian and Hamiltonian densities are computed to third order (in the wave displacement field). An application of these results to study the interaction of gravity waves (g-modes) in white dwarfs stars will be the subject of future work.

Chapter 1 References

Ando, H., and Osaki, Y. 1975, *Publ. Astron. Soc. Japan* **27**, 581.

Biermann, L. 1946, *Naturwiss.* **23**, 118.

Biermann, L. 1947, *Z. Ap.* **25**, 161.

Brown, T. M., Mihalas, B. W., and Rhodes, E. J., Jr. 1986, in *Physics of the Sun*, Vol. I, *The Solar Interior*, eds. P. A. Sturrock, T. E. Holzer, D. M. Mihalas, and R. K. Ulrich (Dordrecht: Reidel).

Christensen-Dalsgaard, J. 1988, in *IAU Symposium 123, Advances in Helio- and Asteroseismology*, eds. J. Christensen-Dalsgaard and S. Frandsen (Dordrecht: Reidel), p. 3.

Christensen-Dalsgaard, J., Duvall, T. L., Jr., Gough, D. O., Harvey, J. W., and Rhodes, E. J., Jr. 1985, *Nature* **315**, 378.

Claverie, A., Isaak, G. R., McLeod, C. P., van der Raay, H. B., and Roca Cortés, T. 1979, *Nature* **282**, 591.

Deubner, F. -L. 1975, *Astron. Astrophys.* **44**, 371.

Deubner, F. -L., and Gough, D. 1984, *Annu. Rev. Astron. Astrophys.* **22**, 593.

Evans, J. W. , and Michard, R. 1962, *Ap. J.* **138**, 493.

Fernandes, D. N. 1992, *The Detection and Characterization of High Frequency and High Wavenumber Solar Oscillations*, Ph.D. Thesis, Stanford.

Goldreich, P., and Keeley, D. A. 1977, *Ap. J.* **212**, 243.

Goldreich, P., and Kumar, P. 1988, *Ap. J.* **326**, 462.

Goldreich, P., and Kumar, P. 1990, *Ap. J.* **363**, 694.

Goldreich, P., and Kumar, P. 1991, *Ap. J.* **374**, 366.

Goldreich, P., and Murray, N. 1994, *Ap. J.* **424**, 480.

Goldreich, P., Murray, N., and Kumar, P. 1994, *Ap. J.* **424**, 466.

Grec, G., Fossat, E., and Pomerantz, M. 1980, *Nature* **288**, 541.

Kaufman, J. M. 1991, *Frequencies and Amplitudes of High Degree Solar Oscillations*, Ph.D. Thesis, Caltech.

Kumar, P. 1988, *Excitation and Damping of Solar P-Modes*, Ph.D. Thesis, Caltech.

Kumar, P., Franklin, J., and Goldreich, P. 1988, *Ap. J.* **328**, 879.

Kumar, P., and Goldreich, P. 1989, *Ap. J.* **342**, 558.

Leibacher, J. W., and Stein, R. F. 1971, *Astrophys. Lett.* **7**, 191.

Leighton, R. B., Noyes, R. W., and Simon, G. W. 1962, *Ap. J.* **135**, 474.

Libbrecht, K. G. 1988, *Space Sci. Rev.* **47**, 275.

Libbrecht, K. G., and Woodard, M. F. 1991, *Science* **253**, 152.

Lighthill, M. J. 1952, *Proc. Roy. Soc. A* **211**, 564.

Lighthill, M. J. 1954, *Proc. Roy. Soc. A* **222**, 1.

Morton, B. R., Taylor, G. I., and Turner, J. S. 1956, *Proc. Roy. Soc. A* **234**, 1.

Musielak Z. E., Rosner R., Stein R. F., and Ulmschneider, P. 1994, *Ap. J.* **423**, 474.

Prandtl, L. 1952, *Essentials of Fluid Dynamics* (London: Blakie).

Proudman, J. 1952, *Proc. Roy. Soc. A* **214**, 119.

Schmidt, W. 1941, *Z. Angew. Math. Mech.* **21**, 265.

Shibahashi, H. 1990, in *Progress of Seismology of the Sun and Stars*, eds. Y. Osaki and H. Shibahashi (Berlin: Springer-Verlag), p. 3.

Spruit, H. C., Nordlund, Å., and Title, A. M. 1990, *Annu. Rev. Astron. Astrophys.* **28**, 263.

Stein, R. F. 1967, *Solar Phys.* **2**, 385.

Stein, R. F., and Leibacher, J. W. 1974, *Annu. Rev. Astron. Astrophys.* **12**, 407.

Stein, R. F., and Nordlund, Å. 1989, *Ap. J.* **342**, L95.

Stix, M. 1989, *The Sun: An Introduction* (Berlin: Springer-Verlag).

Taylor, G. I. 1945, *Dynamics of a Mass of Hot Gas Rising in Air (US AEC MDDC 919, LDAC 276).*

Ulrich, R. K. 1970, *Ap. J.* **162**, 993.

Zirin, H. 1988, *Astrophysics of the Sun* (New York: Cambridge University Press).

CHAPTER 2

Acoustic Radiation of a Buoyant Sphere

The radiation field of a buoyant oscillating sphere is calculated as a model for the excitation of the solar p-modes. Explicit solutions are given in both the near and far fields in the dual limit of small radius (compared to scaleheight) and low pulsation frequency (compared to acoustic cutoff). For frequencies $\omega \lesssim \omega_{AC}$, the energy flux into the p-modes is of order $O((\frac{\omega}{\omega_{AC}})^4)$ relative to the flux from a pure monopole source.

2.1 Introduction

The generation of sound by turbulence is a well-studied problem in both uniform (Lighthill (1952,1954); Proudman (1952)) and gravitationally stratified media (Stein (1967); Goldreich and Kumar (1988); Bogdan *et al.* (1993); Musielak *et al.* (1994)). The latter is important in the study of the excitation of the solar p-modes (Goldreich and Keeley (1977); Goldreich and Kumar (1990); Goldreich, Murray and Kumar (1994)). Calculation of emission spectra is done by Lighthill's method (Lighthill (1952)) which involves the solution of an inhomogeneous wave equation, the source terms of which are modeled and classified according to relative strength. In the case of a stratified atmosphere, these include a monopole term from changes in fluid volume, a dipole term due to changes in external momentum (the resulting buoyancy oscillation), and a quadrupole term from the redistribution of internal momentum (fluctuations in the Reynolds stress).

Other classification schemes referring to the far field radiation patterns or

the order of differentiation in the terms (Musielak 1987) are inappropriate due to the anisotropic propagation in the layered atmosphere and ambiguity concerning the choice of variables. Moreover, in a stably stratified atmosphere, the monopole and dipole contributions are difficult to separate as distinct effects. If a fluid element expands and contracts (monopole excitation), the buoyancy force causes it to rise and fall (dipole excitation). In addition, if the pulsation frequency is small compared to the acoustic cutoff, the element will move so as to maintain approximate hydrostatic equilibrium. In that case, the bobbing amplitude is miraculously tuned to cancel the original monopole radiation in the far field, resulting in a combined amplitude on the same order as the quadrupole term (Goldreich and Kumar (1990)). The implication is that turbulent excitation of low frequency modes is strongly frequency dependent and smaller in magnitude than the independent contributions of the pure monopole and dipole terms. These features are clearly seen in the power spectra of the solar p-modes (see Libbrecht and Woodard (1991)).

The cancellation of the two lowest order poles appears naturally if one uses Lighthill's method and performs a mode expansion as in Goldreich and Kumar (1990), or if one integrates over a persistent, monochromatic source (Appendix 2.1). In addition, these calculations show that the f-mode is not excited by the monopole or dipole processes, a result which depends on the fact that the mode is incompressible. In this Chapter, further evidence for the cancellation is provided by solving a boundary value problem in which the displacement is specified at the surface of a sphere oscillating at fixed frequency ω. The radiation field produced by the oscillating bubble is found by explicit solution of the homogeneous wave equation. We note that a related problem has been considered by Longuet-Higgens (1989a, 1989b, 1990) who studied the underwater emission of sound from raindrops.

The remaining sections of the chapter are organized as follows. In section 2.2, the statement of the problem is given, with a discussion of the solution

by a Boundary Integral Method and matched asymptotic expansions. Section 2.3 includes a derivation and discussion of the acoustic Green's Function for a polytropic atmosphere. Lowest order solutions are offered in section 2.4 for the case of the pure monopole, the pure dipole and the 'buoyant monopole' (mixed monopole and dipole). Finally, in section 2.5, our conclusions are presented and Appendices $A2.1 - A2.5$ give some related results and background.

2.2 Statement of the Problem

We seek an equation describing the behavior of infinitesimal adiabatic disturbances (sound waves). Fluid motions are governed by the Navier-Stokes equations

$$\rho \frac{d\mathbf{v}}{dt} = -\nabla p + \mathbf{F} \tag{2.1a}$$

$$\frac{d\rho}{dt} = -\rho \nabla \cdot \mathbf{v}, \tag{2.1b}$$

where $\mathbf{F}, \mathbf{v}, \rho$ and p are the external force, fluid velocity, density, and pressure, respectively. To close the system, we adopt a constant Γ equation of state for the fluid

$$\frac{(s - s_0)}{c_v} = \log p\rho^{-\Gamma}, \tag{2.2}$$

where s is entropy, c_v is the constant volume specific heat, and s_0 is a constant. For isentropic motions, no energy equation is required for the system.

In our model, the unperturbed medium is a static, plane-parallel polytrope occupying the half space $z > 0$, with the depth coordinate z increasing below the surface. The only external force is gravity $\mathbf{F} = \rho g \hat{\mathbf{z}}$ (g is a constant). Hydrostatic equilibrium gives $\rho \propto z^m, p \propto z^{m+1}$, and $s \equiv const.$, where $m = 1/(\Gamma - 1)$ is the polytropic index. Finally, we define a scaleheight $H = dz/d(\log \rho) = z/m$ and the sound speed $c = \sqrt{gH}$.

Linearization and manipulation of equations (2.1) - (2.2) leads to an inhomogeneous wave equation (Goldreich and Kumar (1990))

$$\nabla^2 Q - \frac{1}{c^2}\frac{\partial^2 Q}{\partial t^2} + \frac{1}{H}\frac{\partial Q}{\partial z} = -\left(\frac{\partial^2 \sigma}{\partial t^2} + \frac{g}{\rho}\frac{\partial(\rho\sigma)}{\partial z}\right) \tag{2.3}$$

in the adiabatic part of the Eulerian enthalpy perturbation

$$Q \equiv \frac{\delta p}{\rho}. \tag{2.4}$$

Q is a convenient choice for a scalar wave variable, from which the displacement field

$$\boldsymbol{\xi} = \frac{1}{\omega^2}\nabla Q + \frac{g}{\omega^2}\sigma\hat{\mathbf{z}} \tag{2.5}$$

may be computed.

The right-hand side of (2.3) consists of source terms which depend linearly on the Eulerian entropy perturbation

$$\sigma \equiv \frac{\delta s}{c_p}. \tag{2.6}$$

One identifies them as the monopole

$$\Sigma_M = -\frac{\partial^2 \sigma}{\partial t^2} \tag{2.7a}$$

and dipole

$$\Sigma_D = -\frac{g}{\rho}\frac{\partial(\rho\sigma)}{\partial z} \tag{2.7b}$$

source terms. The quadrupole term is non-linear and does not appear in our linearized equations. (See Goldreich and Kumar (1990) for a discussion of this term.)

For a localized source, the disturbance is adiabatic (i.e., $\sigma \equiv 0$) outside the excitation region. In this case, the wave equation (2.3) becomes homogeneous, and the excitation problem can be given a boundary value treatment. Assuming the wave variables have a time dependence of the form $\exp(-i\omega t)$, $\omega > 0$, the wave equation becomes

$$\nabla^2 Q + \frac{1}{H}\left(\frac{\partial Q}{\partial z} + \frac{\omega^2}{g}Q\right) = 0. \tag{2.8}$$

Our goal is to solve (2.8) in the half space $z > 0$ external to the region B_0, a sphere of radius R_s located at depth z_s, with some component of ∇Q (i.e., the

displacement field) specified on ∂B_0. At the top of the atmosphere, the Lagrangian pressure perturbation, Δp, must vanish, yielding a self-adjoint boundary condition for Q at $z = 0$:

$$\frac{\Delta p}{\rho} = \frac{\delta p}{\rho} + \frac{\boldsymbol{\xi} \cdot \nabla p}{\rho} = (Q + \frac{g}{\omega^2} Q_z)\Big|_{z=0} = 0. \tag{2.9}$$

In addition, we require $\sqrt{\rho} Q$ to be square integrable in z (so the radiated energy is finite), as well as a radiation condition for outgoing waves as $|R_\perp| \to \infty$.

To find a solution for the given boundary data, we employ the Green's function $G(\mathbf{r}|\mathbf{r}')$ which satisfies

$$\nabla^2 G + \frac{1}{H}\left(\frac{\partial G}{\partial z} + \frac{\omega^2}{g} G\right) = \delta(\mathbf{r} - \mathbf{r}') \tag{2.10}$$

together with the boundary condition at the top of the atmosphere

$$\left(G + \frac{g}{\omega^2} G_z\right)\Big|_{z=0} = 0, \tag{2.11}$$

and the appropriate radiation condition as $|R_\perp| \to \infty$. The quantity $\rho(\mathbf{r}) G(\mathbf{r}|\mathbf{r}')$ is the pressure field of a unit point source located at $\mathbf{r} = \mathbf{r}'$, and it is symmetric with respect to interchange of $\mathbf{r}$ and $\mathbf{r}'$.

If $Q(\mathbf{r})$ is a solution to (2.8), then one can show that

$$\nabla_{\mathbf{r}} \cdot (\rho(\mathbf{r})(Q(\mathbf{r}) \nabla_{\mathbf{r}} G(\mathbf{r}|\mathbf{r}') - G(\mathbf{r}|\mathbf{r}') \nabla_{\mathbf{r}} Q(\mathbf{r}))) = \rho(\mathbf{r}) Q(\mathbf{r}) \delta(\mathbf{r} - \mathbf{r}'), \tag{2.12}$$

for any Green's function $G(\mathbf{r}|\mathbf{r}')$. Integrating over all space, and omitting the vanishing surface terms, one has a solution

$$\rho(\mathbf{r}) Q(\mathbf{r}) = R_s^2 \int_{4\pi} d\Omega' \rho(R_s, \Omega') \times \tag{2.13}$$

$$\left\{ \frac{\partial Q}{\partial r'}(R_s^+, \Omega') G(R_s, \Omega'|\mathbf{r}) - Q(R_s, \Omega') \frac{\partial G}{\partial r'}(R_s^-, \Omega'|\mathbf{r}) \right\}.$$

The $\pm$ superscripts indicate the direction from which derivatives must be evaluated. Equation (2.13) can be used to give the solution anywhere in terms of

the boundary data. Admissible boundary conditions on ∂B_0 include specification of either Q or its normal derivative $\partial Q/\partial r$, or some linear combination of the two, but not both. Given any Green's function, one can always construct another which satisfies the Dirichlet or Neumann Boundary Conditions on ∂B_0 (Appendix 2.2), appropriate to the former two cases. Alternatively, rather than construct the correct Green's function, using *any* such function, one may evaluate (2.13) on the surface and solve it as a Boundary Integral Equation in $Q(\Omega)$ (if $\partial Q/\partial r$ is known on ∂B_0). Once both Q and $\partial Q/\partial r$ are known on the boundary, (2.13) can be used to compute Q elsewhere. Both methods require solving an integral equation, but since care must be taken with the singularities of the Green's function, the latter is easier.

The calculation of the Green's function is crucial to the solution of this problem. Although no exact solution is available in closed form, one needs only the asymptotic behavior of G in the near field (for the static solution of the Boundary Integral Equation), and in the far field (to evaluate the amplitudes of the excited modes). Solutions in the two regions are connected by matching the asymptotic expansions. The next section is devoted to the task of calculating the polytropic Green's function in these limits.

2.3 The Polytropic Acoustic Green's Function

To find the polytropic acoustic Green's function, we perform a 2d Fourier transform on equation (2.10):

$$\hat{G}(\mathbf{k}_\perp, z|\mathbf{R'}_\perp, z') = \iint \frac{d^2\mathbf{R}_\perp}{2\pi} e^{i\mathbf{k}_\perp\cdot\mathbf{R}_\perp} G(\mathbf{R}_\perp, z|\mathbf{R'}_\perp, z'), \tag{2.14}$$

which yields an inhomogeneous equation for $\hat{G}$

$$\hat{G}_{zz} - k_\perp^2\hat{G} + \frac{1}{H}\left(\hat{G}_z + \frac{\omega^2}{g}\hat{G}\right) = \frac{e^{i\mathbf{k}_\perp\cdot\mathbf{R'}_\perp}}{2\pi}\delta(z-z'). \tag{2.15}$$

Solutions to the homogeneous version of (2.15) can be expressed in terms of Kummer functions (confluent hypergeometric functions). One choice of linearly

independent solutions is

$$Q^{(1)} = e^{-k_\perp z} M(a, m, 2k_\perp z) \tag{2.16a}$$

and

$$Q^{(2)} = e^{-k_\perp z} U(a, m, 2k_\perp z), \tag{2.16b}$$

where we define $a \equiv \frac{m}{2}(1 - \omega^2/gk_\perp)$ for $k_\perp = |\mathbf{k}_\perp| > 0$. Other choices exist (see Abramowitz and Stegun (1972)), but (2.16ab) is convenient for several reasons. The Wronskian of these solutions is

$$W(Q^{(1)}, Q^{(2)}) = Q^{(1)} \frac{dQ^{(2)}}{dz} - Q^{(2)} \frac{dQ^{(1)}}{dz} = -\frac{\Gamma(m)}{\Gamma(a)} \frac{2k_\perp}{(2k_\perp z)^m}, \tag{2.17}$$

so they are linearly independent except for wave numbers for which $a = -n$, $n = 0, 1, 2, \ldots$. These coincide with the allowed wavelengths for the p-modes (for fixed frequency)

$$k_\perp = k_n = \frac{\omega^2}{g(1 + \frac{2n}{m})}, \quad n = 0, 1, 2, \ldots. \tag{2.18}$$

The case $n = 0$ is commonly called the f-mode. For $k_\perp = k_n$, both solutions (2.16ab) behave like

$$Q^{(1,2)} \propto e^{-k_n z} L_n^{m-1}(2k_n z), \tag{2.19}$$

where L_n^α is the associated Laguerre polynomial. In this plane-parallel model, these are the eigenfunctions of the p-modes. In Appendix 2.3 we show that they are orthogonal, and the proper normalization is

$$Q_n(z) = \sqrt{\frac{2g}{m\omega^2}} k_n (2k_n)^{m/2} \left(\frac{n!}{\Gamma(m+n)} \right)^{1/2} e^{-k_n z} L_n^{m-1}(2k_n z) \tag{2.20}$$

Although the functions Q_n satisfy the upper boundary and integrability conditions, they do not form a complete set (see Appendix 2.3). Indeed, the closure relation must include a sum over continuum states $k_\perp \neq k_n$. Finally, the solution linearly independent to (2.19) is

$$(2k_\perp z)^{1-m} e^{-k_\perp z} M(1 - m - n, 2 - m, 2k_\perp z), \tag{2.21}$$

but it behaves badly as $z \to 0$ *and* as $z \to \infty$.

Away from these singularities ($k_\perp \neq k_n$), there is no solution which can satisfy both boundary conditions. $Q^{(1)}$ is appropriate for $z \to 0$ as

$$Q^{(1)} \sim 1 - \frac{\omega^2}{g} z, \quad z \to 0, \tag{2.22a}$$

while $Q^{(2)}$ diverges there

$$Q^{(2)} \sim \frac{1}{(2k_\perp z)^{m-1}}, \quad z \to 0. \tag{2.22b}$$

On the other hand, $Q^{(2)}$ is well-behaved as $z \to \infty$

$$Q^{(2)} \sim \frac{1}{(2k_\perp z)^a} e^{-k_\perp z}, \quad z \to \infty, \tag{2.22c}$$

while $Q^{(1)}$ is not integrable

$$Q^{(1)} \sim e^{k_\perp z} (2k_\perp z)^{a-m}, \quad z \to \infty. \tag{2.22d}$$

However, in applications for which a boundary condition at some finite z occurs, these continuum states will be featured in the solution.

The solution to (2.15) for arbitrary $k_\perp$ is proportional to

$$\hat{G}_{||}(k_\perp, z|z') = \frac{Q^{(1)}(z_<) Q^{(2)}(z_>)}{W(Q^{(1)}, Q^{(2)})(z')}, \tag{2.23}$$

where $z_> = \max(z, z')$ and $z_< = \max(z, z')$. A particular solution to (2.10) is given by the inverse Hankel Transform

$$G(\mathbf{r}|\mathbf{r}') = \frac{1}{2\pi} \int_0^\infty dk_\perp k_\perp J_0(k_\perp \tilde{R}) \hat{G}_{||}(|k_\perp|, z|z'), \tag{2.24}$$

where $\tilde{R} = (R^2 + R'^2 - 2\cos(\phi - \phi'))^{1/2}$. To perform the integral (2.24), we make use of the identity relating the Bessel and Hankel functions

$$J_0(z) = \frac{1}{2}(H_0^{(1)}(z) + H_0^{(2)}(z)), \tag{2.25}$$

and formally separate the integral (2.24) into two terms. The first integral passes under the positive real k axis, closing above around the first quadrant, while second must close below encompassing the fourth quadrant. This interpretation insures that the radiation condition is satisfied. Both integrals give a continuum contribution to G, but the first closes around an infinite number of simple poles along the positive real axis, yielding a *modal* contribution. To see this, notice that the integrand is proportional to

$$\Gamma(a) = \Gamma(a,1) + \sum_{n=0}^{\infty} \frac{(-1)^n}{n!} \frac{k_n k_\perp}{k_\perp - k_n} \cdot \frac{2g}{m\omega^2}, \tag{2.26}$$

and the incomplete Γ function is well-behaved over the range of the integration.

The reason both modes and continuum appear in the Green's function has to do with the fact that the eigenvalues vanish as $n \to \infty$. The closure relation for the Sturm-Liouville system (2.8) is of the form

$$\delta(z-z') = \sum_{n=0}^{\infty} Q_n(z)Q_n(z')w(z') \quad + \quad \int dk_\perp A(k_\perp)Q^{(1)}(z_<)Q^{(2)}(z_>)w(z'), \tag{2.27}$$

where $w(z) = z^m$ is the weight function (proportional to the density). This type of closure is typical of systems whose 'potentials' vanish at ∞ (e.g., for the hydrogen atom in quantum mechanics).

It follows that we can partition the Green's function as the sum of two terms

$$G(\mathbf{r}|\mathbf{r}') = G_M(\mathbf{r}|\mathbf{r}') + G_C(\mathbf{r}|\mathbf{r}'), \tag{2.28}$$

where G_M is the modal contribution

$$G_M(\mathbf{r}|\mathbf{r}') = \frac{\pi}{2i} \sum_{n=0}^{\infty} H_0^{(1)}(k_n\tilde{R})Q_n(z)Q_n(z')w(z'), \dagger \tag{2.29}$$

---

† Here we interpret $H_0^{(1)}(k_n\tilde{R}) = \sum_{q=-\infty}^{\infty} J_q(k_nR_<)H_q^{(1)}(k_nR_>)e^{iq(\phi-\phi')}$, with $R_< = \min(R,R')$ and $R_> = \max(R,R')$. This makes the calculation of the azimuthally averaged Green's function easy to compute and assures proper behavior of the solution for all R.

and G_C is the continuum contribution. We have no expression for $G_C(\mathbf{r},\mathbf{r}')$ in closed form. Fortunately, we need only its stationary behavior ($\omega^2 \to 0$) to solve the Boundary Integral Equation.

When the source is of size $R_s \ll g/\omega^2$, and at depth $z_s \lesssim g/\omega^2$, only the continuum contributes to the Green's function. This defines the near field, or the static zone. The shortest wavelength which the modes can accommodate is g/ω^2 (for the f-mode). In addition, in this limit, $|G_M|$ is of order

$$|G_M| = O((\frac{\omega^2 R_s}{g})^{m+1} \ln(\frac{\omega^2 R_s}{g}))|G_C|, \tag{2.30}$$

so it can be neglected when solving the Boundary Integral Equation.

To get the behavior of $G(\mathbf{r}|\mathbf{r}')$ in the near field, we perform an asymptotic expansion around the static point ($\omega^2 \to 0$)

$$G(\mathbf{r}|\mathbf{r}') \sim G_0(\mathbf{r}|\mathbf{r}') + \omega^2 G_1(\mathbf{r}|\mathbf{r}') + \ldots, \tag{2.31}$$

with

$$G_0(\mathbf{r}|\mathbf{r}') = \lim_{\omega^2 \to 0} G(\omega^2; \mathbf{r}|\mathbf{r}'). \tag{2.32}$$

The expansion is only good to order $(\omega^2)^{m+1} \ln(\omega^2)$, after which the modal part of the Green's function must be included. It is well-known that all of the singularities of a wave-like Green's function are contained in the static part of the solution (see Dawson and Fawcett (1990)).

The function G_0 is a solution to

$$\nabla^2 G_0 + \frac{1}{H}\frac{\partial G_0}{\partial z} = \delta(\mathbf{r} - \mathbf{r}'), \tag{2.33}$$

with the approximate boundary condition

$$\left.\frac{\partial G_0}{\partial z}\right|_{z=0} = 0. \tag{2.34}$$

The solution has transform

$$\hat{G}_0 = -\frac{1}{2\pi} e^{i\mathbf{k}_\perp \cdot \mathbf{R}'_\perp} z' \left(\frac{z'}{z}\right)^{\frac{m-1}{2}} I_{\frac{m-1}{2}}(k_\perp z_<) K_{\frac{m-1}{2}}(k_\perp z_>). \tag{2.35}$$

Inverting (2.35), an exact expression for G_0 is found to be

$$G_0(\mathbf{r}|\mathbf{r}') = -\frac{1}{2\pi z}\left(\frac{z'}{z}\right)^{\frac{m-1}{2}} \frac{e^{-\pi i/2}}{\sqrt{2\pi}} \frac{Q^{1/2}_{\frac{m-2}{2}}\left(\frac{z^2+z'^2+\tilde{R}^2}{2zz'}\right)}{\left(\left(\frac{z^2+z'^2+\tilde{R}^2}{2zz'}\right)^2-1\right)^{1/4}}, \tag{2.36}$$

where $Q^{1/2}_{\nu}$ is an associated Legendre Polynomial of the second kind. To manipulate (2.36) into a useful form, define

$$\cosh\alpha = \frac{z^2+z'^2+\tilde{R}^2}{2zz'} \geq 1 \tag{2.37}$$

and

$$\overline{\mathbf{r}'} = \mathbf{r}' - 2z'\hat{\mathbf{z}}. \tag{2.38}$$

$\overline{\mathbf{r}'}$ is the image source point at $z = -z'$. Using the relation

$$Q^{1/2}_{\nu-1/2}(\cosh\alpha) = e^{\pi i/2}\sqrt{\frac{\pi}{2}}\frac{e^{-\nu\alpha}}{\sqrt{\sinh\alpha}}, \tag{2.39}$$

we obtain

$$G_0(\mathbf{r}|\mathbf{r}') = -\frac{1}{4\pi z}\left(\frac{z'}{z}\right)^{\frac{m-1}{2}} \frac{e^{-\frac{m-1}{2}\alpha}}{\sinh\alpha}. \tag{2.40}$$

This can be manipulated to the form

$$G_0(\mathbf{r}|\mathbf{r}') = -\frac{1}{4\pi}(2z')^m \frac{(|\mathbf{r}-\mathbf{r}'|+|\mathbf{r}-\overline{\mathbf{r}'}|)^{1-m}}{|\mathbf{r}-\mathbf{r}'|\,|\mathbf{r}-\overline{\mathbf{r}'}|}, \tag{2.41}$$

or equivalently

$$G_0(\mathbf{r}|\mathbf{r}') = -\frac{1}{4\pi}\frac{(|\mathbf{r}-\mathbf{r}'|-|\mathbf{r}-\overline{\mathbf{r}'}|)^m}{(2z)^m}\left\{\frac{1}{|\mathbf{r}-\mathbf{r}'|}+\frac{1}{|\mathbf{r}-\overline{\mathbf{r}'}|}\right\}. \tag{2.42}$$

For the case $m = 0$, (2.42) shows that G_0 indeed approaches the half-space uniform medium static Green's function (see Appendix 2.5). (2.41) shows that $G_0(\mathbf{r}|\mathbf{r}') \propto w(z')$, as we expect from the above discussion of G_M. Finally, we see from (2.41) that G_0 will not contribute to the far field.

In performing the Boundary Integrals on axisymmetric data, the ϕ dependence is trivial. Unfortunately, the azimuthal average of G_0 is difficult to

obtain without approximation or resorting to numerical integration. For use in later calculations, we expand $G_0(\mathbf{r}|\mathbf{r}')$ in the limit of small R_s/z_s:

$$G_0(\mathbf{r}|\mathbf{r}') = -\frac{1}{4\pi}\frac{1}{|\mathbf{r}-\mathbf{r}'|} - \frac{m}{8\pi}\frac{(r'\mu' - r\mu)}{|\mathbf{r}-\mathbf{r}'|z_s} - \frac{(1-m)}{8\pi z_s} + O(\frac{R_s}{z_s^2}). \tag{2.43}$$

Hence, to first order in R_s/z_s, the azimuthal average is trivial, noting that

$$-\frac{1}{4\pi}\int_0^{2\pi} d\phi \frac{1}{|\mathbf{r}-\mathbf{r}'|} = -\frac{1}{2}\sum_{l=0}^{\infty}\frac{r_<^l}{r_>^{l+1}}P_l(\mu)P_l(\mu'), \tag{2.44}$$

where $r_> = \max(r, r')$ and $r_< = \max(r, r')$.

There are several ways to get the higher order terms in the static expansion (2.31). First, we could write an exact relation

$$G(\mathbf{r}|\mathbf{r}') = G_0(\mathbf{r}|\mathbf{r}') + G_E(\omega^2; \mathbf{r}|\mathbf{r}'), \tag{2.45}$$

with $\hat{G}_E$ given by

$$\hat{G}_E(\omega^2; \mathbf{k}_\perp, z|\mathbf{r}') = -\frac{\omega^2 m}{g}\int_0^{\infty}\frac{dz''}{z''}\hat{G}_0(\mathbf{k}_\perp, z''|\mathbf{r}')\hat{G}_{||}(k_\perp, z|z''). \tag{2.46}$$

Careful treatment of (2.46) shows that

$$\lim_{z\to 0}(\hat{G}_0 + \hat{G}_E) + \frac{g}{\omega^2}\left(\frac{\partial \hat{G}_0}{\partial z} + \frac{\partial \hat{G}_E}{\partial z}\right) = 0. \tag{2.47}$$

Alternatively, we could solve the sequence of problems for the terms in the expansion with

$$\nabla^2 G_n + \frac{1}{H}\frac{\partial G_n}{\partial z} = -\frac{1}{gH}G_{n-1}, \quad n = 1, 2, 3, \ldots, \tag{2.48}$$

and boundary conditions

$$\left.\frac{\partial G_n}{\partial z}\right|_{z=0} = -\frac{1}{g}G_{n-1}(0). \tag{2.49}$$

The recursive solution shows that this is a Born Expansion

$$G_n(\mathbf{r}|\mathbf{r}') = -\frac{1}{g}\int\limits_{z>0} dV'' \frac{d\ln\rho}{dz''} G_0(\mathbf{r}|\mathbf{r}'')G_{n-1}(\mathbf{r}''|\mathbf{r}'). \tag{2.50}$$

Notice from (2.41) that $\rho G_0 = O(1/z)$ as $z \to \infty$, and $G_0 = O(1/R^{m+1})$ as $R \to \infty$, so the surface integrals we cast away in deriving (2.50) do vanish, at least for G_1. In Fourier space, the solution is

$$\hat{G}_n(\mathbf{k}_\perp, z|\mathbf{r}') = -\frac{m}{g}\int\limits_0^\infty \frac{dz''}{z''}\hat{G}_{n-1}(\mathbf{k}_\perp, z''|\mathbf{R}'_\perp, z')\cdot 2\pi e^{-i\mathbf{k}_\perp\cdot\mathbf{R}'_\perp}\cdot\hat{G}_0(\mathbf{k}_\perp, z|\mathbf{R}'_\perp, z''). \tag{2.51}$$

Fortunately, we only need G_0 to get the solution to lowest order if $\omega^2 \ll \omega_{AC}^2$. ($\omega_{AC}$ is the acoustic cutoff at the top of the atmosphere $\sim c/H$.) The next section uses these approximate expressions for the Green's function to obtain solutions to the problems of the pure monopole, pure dipole, and mixed monopole and dipole.

2.4 Lowest Order Solutions

Given the behavior of the Green's function as $|\mathbf{R}_\perp| \sim R_s$ and $|\mathbf{R}_\perp| \to \infty$, we may now solve the Boundary Integral Equation (2.13) to lowest order for some component of the displacement specified on ∂B_0, and estimate the amplitudes of the excited modes. We consider three cases of physical interest.

2.4.1 The Pure Monopole

If the sphere pulsates radially, but is *not* allowed to float up and down, the solution to the Boundary Integral Equation is trivial to lowest order. Keeping only the first term in the static expansion (2.43), we find that Q takes on a value

$$Q(\mu) = -R_s\frac{\partial Q}{\partial r}\bigg|_0 (1 + O(\frac{R_s}{H_s}) + O((\frac{\omega}{\omega_{AC}})^2)). \tag{2.52}$$

In the far field, we use the modal part of the Green's function and obtain

$$Q(R,z) \sim -2\pi^2 i R_s^2 \frac{\partial Q}{\partial r}\bigg|_0 \sum_{n=0}^{\infty} H_0^{(1)}(k_n R)Q_n(z)Q_n(z_s)w(z_s) \tag{2.53}$$

to lowest order. The asymptotic intensity of radiation moving through a cylinder of radius R is given by

$$I = \frac{2\pi R}{2i\omega} \int_0^\infty dz \rho Q^* \frac{\partial Q}{\partial R}. \tag{2.54}$$

By the orthogonality of the modes, we find the intensity on the mode p_n is

$$I_n = M v_r^2 \omega \cdot 3\pi^2 \left(\frac{\omega^2 R_s}{g}\right)\left(\frac{\omega^2 z_s}{g}\right)^m \frac{1}{(1+\frac{2n}{m})^{m+2}} \frac{\Gamma(m+n)}{n!} \tag{2.55}$$

where $M = 4\pi\rho(z_s)R_s^3/3$ and $v_r = \frac{1}{\omega}\frac{\partial Q}{\partial r}\big|_0$. Notice that $I_n \propto 1/n^3$ as $n \to \infty$, so the total intensity is finite.

2.4.2 The Pure Dipole

In this case, the sphere moves rigidly up and down without changing its volume. The solution to this problem in a uniform medium is given in Appendix 2.5. To lowest order in $(\omega^2 H_s/g)$ and R_s/z_s, the near field is the same as in the uniform medium. The first term to contribute to the far field is the dipole one, giving an amplitude smaller by a factor of $(\omega^2 H_s/g)$ than the pure monopole case. To get the exact answer to this order, the correction to the near field Green's function $\omega^2 G_1(\mathbf{r}|\mathbf{r}')$ must be used in solving the Boundary Integral Equation.

2.4.3 The Mixed Monopole and Dipole

In Appendix 2.4, we show that the boundary condition for a buoyant oscillating sphere is

$$\frac{\partial Q}{\partial r}(R_s, \mu) = \frac{\partial Q}{\partial r}\bigg|_0 \left(1 + \frac{3g/R_s}{\omega^2 - g/H_s}\mu\right). \tag{2.56}$$

There are two limits of interest. For high frequencies $\omega^2 \gg g/H_s \sim \omega_{AC}^2$, the sphere is mostly pulsating, with a tiny bobbing motion in phase with the radial motion. At low frequencies, the sphere also bobs, but with a vertical motion out of phase with the expansion. The bubble moves to maintain instantaneous

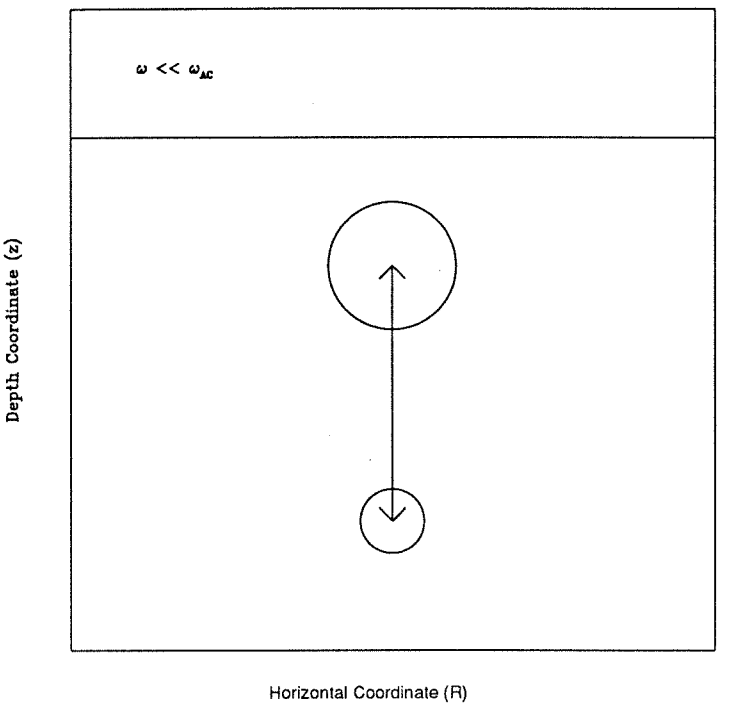

Figure 2.1: A Low Frequency Bubble Oscillation ($\omega \ll \omega_{AC}$). The bubble expands as it rises to maintain approximate hydrostatic equilibrium.

approximate hydrostatic equilibrium. The two types of oscillation are depicted in Figures 2.1 and 2.2.

The boundary condition (2.56) is appropriate only in the limit of small R_s/z_s. This was required to expand the local density contrast in the equation of motion of the sphere. Hence, it is only consistent to seek a solution within the same approximation. We keep the ω^2 dependence of (2.56) throughout the calculation until it is no longer needed to give the lowest order behavior.

It is convenient to rewrite the boundary condition in terms of Legendre polynomials:

$$\rho \frac{\partial Q}{\partial r}(R_s, \mu) = \rho(z_s) \frac{\partial Q}{\partial r}\bigg|_0 \times \tag{2.57}$$

$$\left\{ \frac{\omega^2 H_s}{\omega^2 H_s - g} P_0(\mu) + \left(\frac{R_s}{H_s} + \frac{3gH_s}{R_s(\omega^2 H_s - g)} \right) P_1(\mu) + 2\frac{g}{\omega^2 H_s - g} P_2(\mu) \right\}.$$

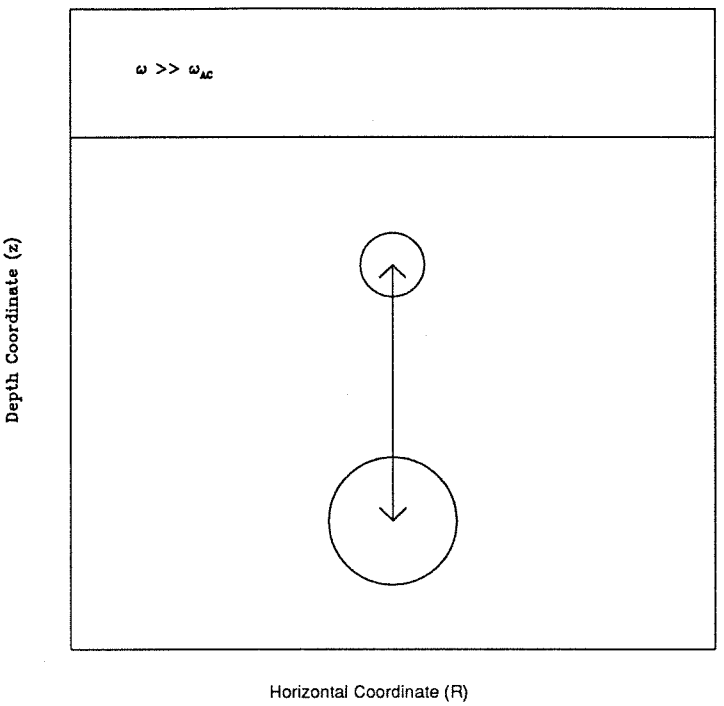

Figure 2.2: A High Frequency Bubble Oscillation ($\omega \gg \omega_{AC}$). The contraction is out of phase with the bubble motion is this case.

Using only the zeroth order in $G_0(\mathbf{r}|\mathbf{r}')$, Q takes a value

$$\rho Q(R_s,\mu) = -R_s\rho(z_s)\frac{\partial Q}{\partial r}\bigg|_0 \times \tag{2.58}$$

$$\left\{\frac{\omega^2 H_s}{\omega^2 H_s - g}P_0(\mu) + \frac{1}{2}\left(\frac{R_s}{H_s} + \frac{3gH_s}{R_s(\omega^2 H_s - g)}\right)P_1(\mu) + \frac{2}{3}\frac{g}{\omega^2 H_s - g}P_2(\mu)\right\}.$$

To calculate behavior of Q in the far field, we expand the eigenfunctions appearing in the modal part of the Green's function, and evaluate them at the surface

$$Q_n(z_s + R_s\mu) \sim Q_n(0)\cdot(1 - \frac{\omega^2 z_s}{g} - \frac{\omega^2 R_s}{g}\mu + O((\frac{\omega}{\omega_{AC}})^2)). \tag{2.59}$$

Although the $P_1(\mu)$ component of the near field may be large, one has to go to order $(\omega/\omega_{AC})^2$ in the eigenfunction to get a contribution to the far field. It follows that the mixed monopole and dipole has an amplitude smaller by a factor of $(\omega/\omega_{AC})^2$ relative to the pure monopole case. As with the pure

dipole, to get a numerical estimate to the implied order, one needs to include the first correction to the static expansion when solving the Boundary Integral Equation.

2.5 Discussion

The purpose of this work was to calculate the radiation field of a localized acoustic source in a gravitationally stratified medium. In addition to developing some new theoretical tools specific to this problem, our main result is a demonstration of the curious cancellation effect when an expanding and contracting fluid element is allowed to float in the external atmosphere. While this important effect was previously appreciated (Goldreich and Kumar (1990)), our approach of treating the excitation as a boundary value problem provides an independent verification, as well as a framework for performing future calculations in similar problems. To the extent that our model applies to convective turbulence is the sun, our results are relevant to the theory of the excitation of solar p-modes.

Certain restrictions must be kept in mind when interpreting these results, and their applicability to practical problems. In order to pose a solvable problem, certain non-physical assumptions were made regarding the nature of the source and the ambient medium. In particular, corrections due to the finite size of the fluid elements, their finite lifetime (transience), non-sphericity and non-adiabaticity may be significant, the latter two being the most problematic, because the underlying assumptions are clearly contrived. Although no resolution of these problems is at hand, we see no reason why they should conflict with our main result, whose interpretation is unambiguous and physically meaningful.

In conclusion, we suggest some future applications for which this work may be relevant. More careful solutions could be found, including corrections of higher order in the static and finite size expansions of the Green's function, and numerical solutions of the Boundary Integral Equation. For example, this

would be necessary to understand the excitation of modes with frequencies up to the acoustic cutoff. In addition, the formalism is applicable to calculations of absorption and scattering of sound waves by standing bubbles.

Appendix 2.1

Cancellation for a Local Source of Entropy Fluctuation

As an alternative method of demonstrating the cancellation effect for a buoyant monopole, consider the following model. The wave equation (2.3) can be solved with a local source of entropy fluctuation confined to a sphere of radius R_s centered at depth $z_s > R_z$. The horizontal boundary of the sphere is given by

$$R(z) = \sqrt{R_s^2 - (z - z_s)^2}, \qquad (A2.1.1)$$

and the vertical boundaries of the sphere occur at depths $z_\pm = z_s \pm R_s$. Taking the horizontal Fourier transform of (2.3), we obtain a second order inhomogeneous wave equation

$$\hat{Q}_{zz} - k_\perp^2 \hat{Q} + \frac{1}{H}\left(\hat{Q}_z + \frac{\omega^2}{g}\hat{Q}\right) = \Sigma = \mathbf{D}\Lambda, \qquad (A2.1.2)$$

where $\mathbf{D} = \omega^2 - \frac{g}{H} - g\partial_z$, and

$$\Lambda(k_\perp, z) = \sigma_0(z)\pi R^2(z)\left[\frac{2J_1(k_\perp R(z))}{k_\perp R(z)}\right]. \qquad (A2.1.3)$$

The solution to $(A2.1.2)$ can be found by using the Green's function, yielding

$$\hat{Q}(k_\perp, z) = \int_z^\infty dz' \frac{Q^{(2)}(z')\Sigma(z')}{W(z')} Q^{(1)}(z) + \int_0^z dz' \frac{Q^{(1)}(z')\Sigma(z')}{W(z')} Q^{(2)}(z), \quad (A2.1.4)$$

where $Q^{(1)}, Q^{(2)}$ and W are described in section 2.3. An integration by parts allows us to write $(A2.1.4)$ in the form

$$\hat{Q}(k_\perp, z) = \int_z^{z_+} dz' \frac{\Lambda(z')(\omega^2 + g\partial_{z'})Q^{(2)}(z')}{W(z')} Q^{(1)}(z) \quad +$$

$$\int_{z_-}^z dz' \frac{\Lambda(z')(\omega^2 + g\partial_{z'})Q^{(1)}(z')}{W(z')} Q^{(2)}(z). \qquad (A2.1.5)$$

The surface terms for each integral cancel one another exactly. Since $Q^{(1)}$ behaves like $(\omega^2 + g\partial_z)Q^{(1)} \sim 0$ near the surface, the mixture of monopole and dipole sources cancel to one higher order in $(\omega^2 H_s/g)$ than either term taken independently. This is essentially the source of the cancellation noted in Goldreich and Kumar (1991). Also notice that the integral vanishes for the wave number of the f-mode, for which $Q + gQ_z/\omega^2 \equiv 0$ for all z.

As a further illustration, consider the limit $R_s \to 0$ for which the bubble becomes a point source. In this case, the source term becomes

$$\Lambda(k_\perp, z) = \sigma_0 e^{i\mathbf{k}_\perp \cdot \mathbf{R}'_\perp} \lambda^3 \delta(z - z_s), \qquad (A2.1.6)$$

where λ^3 is a measure of the source volume. Performing the integrals, one finds

$$Q(k_\perp, z) = -g\sigma_0 \lambda^3 \left[\frac{\Gamma(a)}{\Gamma(m)} (2k_\perp z_s)^m e^{-k_\perp z_s} \right] e^{-k_\perp z} \times \qquad (A2.1.7)$$

$$\left(M'(a, m, 2k_\perp z_s) - \frac{a}{m} M(a, m, 2k_\perp z_s) \right) U(a, m, 2k_\perp z), \quad z > z_s$$

$$\left(U'(a, m, 2k_\perp z_s) - \frac{a}{m} U(a, m, 2k_\perp z_s) \right) M(a, m, 2k_\perp z), \quad z < z_s,$$

where the prime denotes differentiation with respect to the third argument. A similar result is obtained for the extended object in the limit $k_\perp R_0 \ll 1$, with $\lambda^3 = 4\pi R_0^3/3$. The point source has the peculiar property that the top and bottom of the source move in different directions as it expands and contracts, yielding a jump in the displacement. Aside from this, one may verify that the Lagrangian pressure perturbation is continuous across the source. For the continuum wavenumbers ($k_\perp \neq k_n$, the wavenumber for the mode p_n), the solution approximates a white spectrum with

$$|\xi_z| \sim \sigma_0 \lambda^3, \qquad (A2.1.8)$$

for $k_\perp z_s \ll 1$, while for $k_\perp z_s \gtrsim 1$, one has an exponential spectrum

$$|\xi_z| \sim \sigma_0 \lambda^3 e^{-k_\perp z_s}. \qquad (A2.1.9)$$

It is not surprising that a point source produces a broad white continuum down to wavelengths of order the depth of the source. Moreover, a field of randomly distributed sources would also produce such a spectrum. Each source would merely be phase shifted by a factor $e^{i\mathbf{k}_\perp \cdot \mathbf{x}^s_\perp}$, where $\mathbf{x}^s_\perp$ is the horizontal location of the source. In expectation, the amplitude of continuum depends only on the correlation spectrum of the source distribution, which one expects to be flat down to wavelengths of order the mean separation of the sources. The observations presented in Chapter 4 reveal that the spectrum has an exponential shape over a wide range of $k_\perp$.

Appendix 2.2

Construction of a Proper Green's Function

Assume that a certain solution to (2.10), $G_T(\mathbf{r}|\mathbf{r}')$, is known. Then one can always construct a Green's function, $G_D(\mathbf{r}|\mathbf{r}')$, for Dirichlet boundary data on the surface of the sphere ($\partial G_D/\partial r = 0$), as well as a function $G_N(\mathbf{r}|\mathbf{r}')$, applicable to the Neumann Boundary Condition ($G_N = 0$). To calculate $G_N(\mathbf{r}|\mathbf{r}')$ for use in our problem, we note that G_N and G_T satisfy

$$\nabla_{\mathbf{r}} \cdot (G_N(\mathbf{r}|\mathbf{r}')\nabla_{\mathbf{r}} G_T(\mathbf{r}|\mathbf{r}') - G_T(\mathbf{r}|\mathbf{r}')\nabla_{\mathbf{r}} G_N(\mathbf{r}|\mathbf{r}')) =$$

$$\rho(\mathbf{r})\delta(\mathbf{r}-\mathbf{r}')(G_N(\mathbf{r}|\mathbf{r}') - G_T(\mathbf{r}|\mathbf{r}')). \qquad (A2.2.1)$$

Since the outer surface boundary conditions are self-adjoint, the surface terms vanish when ($A2.2.1$) is integrated over all space. Using the symmetry property of the Green's functions

$$\rho(\mathbf{r})G(\mathbf{r}|\mathbf{r}') = \rho(\mathbf{r}')G(\mathbf{r}'|\mathbf{r}), \qquad (A2.2.2)$$

with the boundary condition on G_N on the sphere, the integration yields

$$G_N(\mathbf{r}|\mathbf{r}') = G_T(\mathbf{r}|\mathbf{r}') + R_s^2 \int_{4\pi} d\Omega'' \frac{\rho(\mathbf{r}'')}{\rho(\mathbf{r})} G_T(\mathbf{r}''|\mathbf{r}) \frac{\partial G_N}{\partial r''}(\mathbf{r}''|\mathbf{r}')\Big|_{|\mathbf{r}''|=R_s}. \qquad (A2.2.3)$$

Differentiating ($A2.2.3$) with respect to r, we have a single Boundary Integral Equation from which $\partial G_N/\partial r$ may be computed at $|\mathbf{r}| = R_s$.

Appendix 2.3

Orthonormality of the Basis Functions

In section (2.3) we encounter a homogeneous wave equation of the form

$$\frac{1}{\rho}\frac{\partial}{\partial z}\left(\rho\frac{\partial Q}{\partial z}\right) - k^2 Q + \frac{\omega^2}{gH}Q = 0. \qquad (A2.3.1)$$

There are two interpretations of $(A2.3.1)$ as a Sturm-Liouville system, depending on whether k^2 or ω^2 are held constant. Since our excitation occurs at fixed frequency, we treat k^2 as a variable parameter, with the discrete eigenvalues k_n corresponding to the eigenfunctions Q_n. To show orthogonality of the eigenfunctions, we note that two distinct solutions Q_n, Q_m with $k_n \neq k_m$ satisfy

$$\frac{\partial}{\partial z}\rho\left(\frac{\partial Q_n}{\partial z}Q_m - \frac{\partial Q_m}{\partial z}Q_n\right) = (k_n^2 - k_m^2)\rho Q_n Q_m. \qquad (A2.3.2)$$

Since the boundary condition at $z = 0$ is self-adjoint, integrating $(A2.3.2)$ from $z = 0$ to $z = \infty$, we find

$$\int_0^\infty dz \rho Q_n Q_{n'} = 0 \qquad k_n \neq k_{n'}. \qquad (A2.3.3)$$

The constant frequency eigenfunctions can be expressed as

$$Q_n \propto e^{-k_n z} L_n^{m-1}(2k_n z), \qquad (A2.3.4)$$

where L_n^{m-1} are associated Laguerre polynomials, and the eigenvalues are $k_n = \omega^2/g(1 + 2n/m)$. To normalize, consider the integral

$$I(n,\alpha) = \int_0^\infty dx e^{-x} x^{\alpha+1}(L_n^\alpha)^2 \qquad (A2.3.5)$$

$$= (\alpha + 1 + 2n)\frac{\Gamma(n+\alpha+1)}{n!},$$

from which we compute

$$Q_n(z) = \sqrt{\frac{2g}{m\omega^2}}k_n(2k_n)^{m/2}\left(\frac{n!}{\Gamma(m+n)}\right)^{1/2} e^{-k_n z} L_n^{m-1}(2k_n z) \qquad (A2.3.6)$$

as the normalized eigenfunctions satisfying

$$\int_0^\infty dz z^m Q_n(z) Q_{n'}(z) = \delta_{n,n'}. \qquad (A2.3.7)$$

To see that this set of eigenfunctions is not complete, consider the sum

$$\Delta(z,z') = z^m \sum_{n=0}^{\infty} Q_n(z) Q_n(z'). \qquad (A2.3.8)$$

The sum clearly *converges* since $k_n \propto 1/n$, as $n \to \infty$. Moreover, it is well-behaved for all z, z', including the case $z = z'$. If the above set of eigenfunctions were complete, then the sum $(A2.3.8)$ would behave like a delta function (i.e., a closure relation).

On the other hand, if one takes k^2 to be constant in $(A2.3.1)$, the orthonormal eigenfunctions are

$$\tilde{Q}_n(z) = (2k)^{m/2} \left(\frac{n!}{\Gamma(m+n)} \right)^{1/2} e^{-kz} L_n^{m-1}(2kz) \qquad (A2.3.9)$$

with eigenvalues

$$\omega_n^2 = gk(1 + \frac{2n}{m}). \qquad (A2.3.10)$$

In this case, the closure relation is obtained from the well-known summation identity for the Laguerre polynomials (Gradshteyn and Ryzhik (1994))

$$\sqrt{zz'}^{m-1} \sum_{n=0}^{\infty} \tilde{Q}_n(z) \tilde{Q}_n(z') = \lim_{q \to 1^-} \frac{2k}{1-q} e^{\frac{-2k(z+z')}{1-q}} I_{m-1}(\frac{2\sqrt{2kz}\sqrt{2kz'}}{1-q}) \qquad (A2.3.11)$$

$$= \lim_{\epsilon \to 0} \frac{k}{\sqrt{\pi \epsilon}} e^{-\frac{(\sqrt{2kz} - \sqrt{2kz'})^2}{\epsilon}} \frac{1}{(\sqrt{2kz}\sqrt{2kz'})^{1/2}}$$

$$= 2k \cdot \frac{1}{2} \frac{1}{(\sqrt{2kz}\sqrt{2kz'})^{1/2}} \delta(\sqrt{2kz} - \sqrt{2kz'})$$

$$= \delta(z - z'),$$

so these eigenfunctions are indeed complete.

Appendix 2.4

Boundary Condition for a Buoyant Monopole

Consider a sphere of radius R_s centered at depth $z_s > R_s$. Let the sphere undergo an infinitesimal oscillation in its radius with amplitude ΔR and frequency ω. Finally, assume the radius is small compared to the local scaleheight, H. The change in volume induces a buoyant force on the sphere of magnitude $\Delta\rho g$, where $\Delta\rho = \rho_{\text{sphere}} - \rho_{\text{medium}} = -(3\Delta R/R_s + \Delta z/H_s)\overline{\rho}$, and the center of the sphere is displaced an amount Δz in the vertical direction. Hence, the equation of motion for the sphere is

$$-\omega^2 \Delta z = -3g\frac{\Delta R}{R_s} - g\frac{\Delta z}{H_s} \qquad (A2.4.1)$$

which implies a relation

$$\Delta z = \frac{3g}{R(\omega^2 - g/H_s)}\Delta R. \qquad (A2.4.2)$$

The factor of 3 in the right-hand side of $(A2.4.2)$ is crucial in exhibiting the cancellation of the monopole and dipole. From $(A2.4.3)$ we notice that Δz can be of either sign, for positive ΔR, depending on the magnitude of the dimensionless number $\omega^2 H_s/g$. For low frequencies ($\omega^2 \ll g/H_s \sim \omega_{AC}^2$), the sphere moves to a vertical position of approximate hydrostatic equilibrium, with Δz out of phase with ΔR. For high frequencies, the bobbing motion is in phase with the change in radius, with the amplitude of vertical displacement drastically reduced. In between the extremes lies a resonance at the frequency $\omega^2 = g/H_s$. The two limits are summarized in Figures 2.1 and 2.2.

Although knowledge of Δz and ΔR does not imply a unique boundary condition for the displacement field at the surface of the sphere, the radial component *is* well defined for any infinitesimal motion. Throughout the movement of the bubble, we assume the surface remains spherical in this model. Consider a point on the surface at the beginning of the cycle, located at coordinates

$$z = z_s + R_s\mu \qquad (A2.4.3a)$$

$$R = R_s\nu, \qquad (A2.4.3b)$$

where $\mu = \cos\theta$ and $\nu = \sin\theta$. By symmetry the point slides through some trajectory on the surface of constant ϕ. At the extreme point of the oscillation, it is mapped to a point with coordinates

$$\tilde{z} = z_s + \Delta z + (R_s + \Delta R)\tilde{\mu} \qquad (A2.4.4a)$$

$$\tilde{R} = (R_s + \Delta R)\tilde{\nu}. \qquad (A2.4.4b)$$

The problem is that the mapping $\tilde{\mu}(\mu)$ is not determined in this model, but must be computed by solving the wave equation for the external fluid. In general, the fluid will slip along the spherical surface, and the extent of the slippage is not immediately obvious from the relation $(A2.4.2)$. However, notice that the radial displacement is given by

$$\xi_r = \mu\xi_z + \nu\xi_R = \mu(\tilde{z} - z) + \nu(\tilde{R} - R), \qquad (A2.4.5)$$

which implies that

$$\xi_r = \Delta R + \mu\Delta z + (R_s + \Delta R)(\mu\tilde{\mu} + \nu\tilde{\nu} - 1). \qquad (A2.4.6)$$

The first two terms on the right-hand side of $(A2.4.6)$ are known, while the latter is undetermined. Clearly the slippage is of order

$$\Delta\mu = \tilde{\mu} - \mu = O(\Delta z/R_s) \qquad (A2.4.7a)$$

$$\Delta\nu = \tilde{\nu} - \nu = O(\Delta R/R_s), \qquad (A2.4.7b)$$

so the quantity $\mu\tilde{\mu} + \nu\tilde{\nu} - 1$ is of second order in the displacement. Hence, the boundary condition on ξ_r is uniquely given by

$$\xi_r \approx \Delta R + \mu\Delta z \qquad (A2.4.8)$$

to lowest order in the infinitesmal motions. The degree of slippage can be calculated using $(A2.4.8)$ as a boundary condition. One could then iterate on the

calculated mapping $\tilde{\mu}(\mu)$, but this is not necessary for a linear wave calculation. Alternatively, one could form a non-linear Boundary Integral system and compute the map $\tilde{\mu}(\mu)$ exactly. The existence and uniqueness of the solution are not necessarily guaranteed in this case, however, as with the linear equation (Carrier *et al.* (1983)).

Appendix 2.5

Bubble Radiation in a Uniform Medium

The radiation of a sphere oscillating in a uniform medium is substantially more simple than the polytropic case considered in this paper, because the Green's function may be calculated explicitly. The discussion in this Appendix is mostly motivational, although several of the results presented here are unique to this work or required for some application.

The wave equation for the uniform case is

$$\Delta Q + (\frac{\omega}{c})^2 Q = 0, \qquad (A2.5.1)$$

where c is the uniform sound speed. The Green's functions for the outgoing waves are given by

$$G_s(\mathrm{r}|\mathrm{r}') = -\frac{1}{4\pi}\frac{e^{i\omega/c|\mathrm{r}-\mathrm{r}'|}}{|\mathrm{r}-\mathrm{r}'|} \qquad (A2.5.2)$$

and

$$G_\pm(\mathrm{r}|\mathrm{r}') = -\frac{1}{4\pi}\left(\frac{e^{i\omega/c|\mathrm{r}-\mathrm{r}'|}}{|\mathrm{r}-\mathrm{r}'|} \pm \frac{e^{i\omega/c|\mathrm{r}-\overline{\mathrm{r}'}|}}{|\mathrm{r}-\overline{\mathrm{r}'}|}\right) \qquad (A2.5.3)$$

where

$$\overline{\mathrm{r}'} = \mathrm{r}' - 2z'\hat{\mathrm{z}} \qquad (A2.5.4)$$

is the image point. $(A2.5.2)$ is appropriate for the region R^3, while the $(\pm)$ versions of $(A2.5.3)$ are to be used in the half space $z > 0$ for problems with the boundary conditions $\partial G_+/\partial r = 0$ and $G_- = 0$ at the $z = 0$ line. The functions yield outgoing waves for $\omega > 0$.

The function G_s may be expanded in modes

$$G_s(\mathrm{r}|\mathrm{r}') = \frac{1}{8i}\frac{1}{\sqrt{rr'}}\sum_{l=0}^{\infty}(2l+1)J_{l+1/2}(\frac{\omega r_<}{c})H^{(1)}_{l+1/2}(\frac{\omega r_>}{c})P_l(\cos\gamma) \qquad (A2.5.5)$$

where

$$\cos\gamma = \cos\theta\cos\theta' + \sin\theta\sin\theta'\cos(\phi-\phi') \qquad (A2.5.6)$$

and

$$r_< = \min(r, r') \qquad (A2.5.7a)$$

$$r_> = \max(r, r'). \qquad (A2.5.7b)$$

For axisymmetric problems, the angular average of G_s is needed:

$$\overline{G_s}(\mu, r|\mu', r') = \frac{1}{2\pi}\int_0^{2\pi} d\phi G_s(\mathbf{r}|\mathbf{r}') \qquad (A2.5.8)$$

$$= \frac{1}{8i}\frac{1}{\sqrt{rr'}}\sum_{l=0}^{\infty}(2l+1)J_{l+1/2}(\frac{\omega r_<}{c})H^{(1)}_{l+1/2}(\frac{\omega r_>}{c})P_l(\mu)P_l(\mu'),$$

where $\mu = \cos\theta$. The static part of $\overline{G_s}$ (for $\omega R_s/c \to 0$) may be expressed in terms of elliptical integrals, or as a mode expansion

$$\lim_{\omega\to 0}\overline{G_s}(\omega; \mu, r|\mu', r') = -\frac{1}{2}\sum_{l=0}^{\infty}\frac{r_<^l}{r_>^{l+1}}P_l(\mu)P_l(\mu'). \qquad (A2.5.9)$$

In problems for which $\omega R_s/c \ll 1$ (the period is much longer than the sound travel time across the source), (A2.5.9) is useful for solving the analogous Boundary Integral Equation. Finally, one can always express the solution to the full space problem in the form

$$Q(r, \Omega, t) = e^{-i\omega t}\sum_{l=0}^{\infty}\sum_{m=-l}^{l}\alpha_{lm}\frac{H^{(1)}_{l+1/2}(\frac{\omega r}{c})}{\sqrt{r}}Y_{lm}(\Omega). \qquad (A2.5.10)$$

To obtain solutions to lowest order in $\omega R_s/c$, one uses only the static wave expansion to match the boundary condition on the surface of the sphere. Once the amplitudes of the modes are determined from the boundary data, the far field may be calculated. Three examples of physical interest are now given, all with axisymmetry.

A2.5.1 The case $\left.\frac{\partial Q}{\partial r}\right|_{r=R_s} = AP_l(\mu)$

When the radial displacement is specified on the boundary, the solution is trivial. In the static approximation, the near field is expanded as

$$Q(\mu, r) = \sum_{l'=0}^{\infty} A_{l'} \left(\frac{R_s}{r}\right)^{l'+1} P_{l'}(\mu), \quad r \geq R_s. \tag{A2.5.11}$$

Hence, the expansion coefficients $A_{l'}$ are given by

$$A_{l'} = -\frac{RA}{l'+1}\delta_{l',l}. \tag{A2.5.12}$$

These are the multipole solutions in the normal sense of the word.

The intensity of the far field radiation is

$$I = \Im \frac{1}{2}\rho \int d\mathbf{A} \cdot Q\mathbf{v} \tag{A2.5.13}$$

$$= \frac{\rho\pi r^2}{c} \int_{-1}^{1} d\mu |Q|^2$$

$$I_l = \frac{3}{2} M v_r^2 \omega \left(\frac{\omega R_s}{c}\right)^{2l+1} \left(\frac{\Gamma(3/2)}{\Gamma(3/2+l)}\right)^2 \frac{1}{4^l} \frac{2l+1}{(l+1)^2},$$

where $v_r = A/\omega$ and $M = 4\pi R^3/3\rho$. This example shows the familiar ordering of the multipoles with the dipole being smaller than the monopole by a factor of $(\omega R_s/c)^2$, and the quadrupole by a factor of $(\omega R_s/c)^4$. In addition, the pattern of the radiation in the far field is consistent with the usual meaning of the multipole field. For the non-uniform medium addressed in this paper, neither the order of amplitudes nor the far field radiation pattern are appropriate for classifying the poles.

A2.5.2 The case $\left.\frac{\partial Q}{\partial R}\right|_{r=R_s} = const.$

If the expansion and contraction of the sphere is purely *horizontal*, one can show that the motion is a superposition of all the even multipoles with

$$A_{2l} \sim -\frac{4l+3}{8}\frac{\pi^2}{((l+1)!)^2(\Gamma(1/2-l))^2}R_s\left.\frac{\partial Q}{\partial R}\right|_{r=R_s}, \qquad (A2.5.14)$$

to lowest order in the static limit. In the far field, the dominant contribution is from the monopole term, giving an intensity

$$I = \frac{3}{2}(\frac{3\pi}{8})^2 M\omega v_R^2 \cdot \left(\frac{\omega R_s}{c}\right), \qquad (A2.5.15)$$

of the same order as the simple monopole, and differing only by a factor of $(3\pi/8)^2$.

A2.5.3 The case $\left.\frac{\partial Q}{\partial z}\right|_{r=R_s} = const.$

Finally, we consider the case in which a rigid sphere bobs up and down in the z direction. In this case, one expects the far field to appear as some form of dipole, with the entire pattern consisting of purely odd multipoles. Since the Boundary Integral Equation

$$Q = R_s^2 \int_{4\pi} d\Omega' \left(\frac{\partial Q}{\partial r'}G - Q\frac{\partial G}{\partial r'}\right) \qquad (A2.5.16)$$

requires that we know the normal component of ∇Q at the surface, it cannot be solved in its present form. However, a formal differentiation of $(A2.5.16)$ with respect to R yields an additional equation with which we can close the system

$$\frac{\partial Q}{\partial R} = R_s^2 \int_{4\pi} d\Omega' \left(\frac{\partial Q}{\partial r'}\frac{\partial G}{\partial R} - Q\frac{\partial^2 G}{\partial r' \partial R}\right). \qquad (A2.5.17)$$

Since

$$\frac{\partial Q}{\partial r} = \mu\frac{\partial Q}{\partial z} + \nu\frac{\partial Q}{\partial R}, \qquad (A2.5.18)$$

the coupled system $(A2.5.16-17)$ can be solved for $\partial Q/\partial R$ and Q to obtain the expansion coefficients for evaluating the far field. Writing

$$\Psi = \nu Q_R = \sum_{l=0}^{\infty} \Psi_l P_l(\mu) \qquad (A2.5.19a)$$

and

$$Q = \sum_{l=0}^{\infty} Q_l P_l(\mu), \qquad (A2.5.19b)$$

we find after some manipulation that Q_l and Ψ_l are determined by solving the recursion relations

$$\frac{l+1}{2l+1}Q_l + \frac{1}{2l+1}\Psi_l = -\frac{c}{3}\delta_{l,1} \qquad (A2.5.20a)$$

$$\Psi_l = \frac{2c}{5}(\delta_{l,1} - \delta_{l,3}) - \frac{l(l+1)(l+2)}{(2l+1)(2l+3)}Q_l + \frac{(l+1)(l+2)}{(2l+1)(2l+3)}\Psi_l +$$

$$\frac{l(l-1)(l-2)}{(2l-1)(2l-3)}Q_{l-2} - \frac{l(l-1)}{(2l-1)(2l-3)}\Psi_{l-2}, \qquad (A2.5.20b)$$

where $c = R_s \frac{\partial Q}{\partial z}\Big|_{r=R_s}$ is the known value of the vertical derivative. Solving the system (A2.5.20), one obtains the (static) near field of Q as

$$Q(\mu, r) = -R_s \frac{\partial Q}{\partial z}\Big|_0 \sum_{n=0}^{\infty} (-1)^n \frac{4n+5}{2n+2} \binom{2(n+1)}{n+1} \left(\frac{R_s}{2r}\right)^{2(n+1)} P_{2n+1}(\mu). \qquad (A2.5.21)$$

As expected, only odd multipoles are excited by this motion. To verify that (A2.5.21) indeed satisfies the boundary condition, we evaluate

$$\frac{\partial Q}{\partial z}\Big|_{r=R_s} = \frac{\partial Q}{\partial z}\Big|_0 \sum_{n=0}^{\infty} (-1)^n (4n+5) \binom{2(n+1)}{n+1} \frac{1}{2^{2(n+1)}} P_{2n+2}(\mu) \qquad (A2.5.22)$$

$$= \frac{\partial Q}{\partial z}\Big|_0 [1 - 2\delta(\mu)].$$

The boundary condition is satisfied everywhere except at $\mu = 0$, on the horizontal edge of the sphere where the displacement has infinite shear, also a physically meaningful result. The singularity at $\mu = 0$ is further clarified by manipulating (A2.5.21) to the form

$$Q(\mu, R_s) = -R_s \frac{\partial Q}{\partial z}\Big|_0 \frac{1}{\mu}\left[1 + \sum_{m=0}^{\infty} \frac{96m^3 + 112m^2 + 30m + 17}{4(4m+3)(4m-1)(m+1)^2} P_{2m}(0) P_{2m}(\mu)\right]. \qquad (A2.5.23)$$

The summation in (*A*2.5.23) converges for all μ, so $Q \propto 1/\mu$ as $\mu \to 0$. Evaluating the far field, we obtain

$$Q \sim \frac{5i}{4}\left(\frac{\omega R_s}{c}\right) R_s \frac{\partial Q}{\partial z}\bigg|_0 \left(\frac{R_s}{r}\right) e^{i\omega r/c} P_1(\mu), \qquad (A2.5.24)$$

a dipole field, as anticipated. The asymptotic intensity is also of dipole order

$$I \sim \frac{1}{2} M v_z^2 \omega \left(\frac{\omega R_s}{c}\right)^3 \left(\frac{25}{16}\right). \qquad (A2.5.25)$$

One may object to a boundary condition of the form $\partial Q/\partial z = const.$, since existence and uniqueness theorems require the *normal* component of the derivative to be specified. In fact, the dipole boundary condition does *not* yield a unique solution. For example, a whole family of near field solutions with constant $\partial Q/\partial z$ exist, indexed by $n = 0, 1, ...$

$$Q^{\{n\}} = 2R_s \frac{\partial Q}{\partial z}\bigg|_0 (2n+1)(n+1) \times$$

$$\left[\frac{1}{2n+1} Q_{2n}(\mu)\left(\frac{R_s}{r}\right)^{2n+1} - \right.$$

$$\left. \sum_{m=0}^{\infty} \frac{4m+5}{4(m+1)(m+n+2)(2(m-n)+1)}\left(\frac{R_s}{r}\right)^{2m+2} P_{2m+1}(\mu)\right], \qquad (A2.5.26)$$

where Q_{2n} is a Legendre polynomial of the second kind. Each solution is again odd, but now diverges at $\mu \to \pm 1$. In the far field, these behave as

$$Q^{\{n\}} \sim -\frac{3i}{2}\frac{n+1}{n+2}\frac{\omega R_s}{c} R_s \frac{\partial Q}{\partial z}\bigg|_0 \frac{R_s}{r} e^{i\omega r/c} P_1(\mu), \qquad (A2.5.27)$$

all becoming dipoles (for $\omega R_s/c \ll 1$), and with intensity

$$I^{\{n\}} = \frac{1}{2} M v_z^2 \omega \left(\frac{\omega R_s}{c}\right)^3 \frac{9}{4}\left(\frac{n+1}{n+2}\right)^2. \quad n > 0 \qquad (A2.5.28)$$

There are also a multitude of solutions which are not well-behaved as $r \to \infty$ (i.e., the intensity diverges).

Chapter 2 References

Abramowitz, M., and Stegun, I. A., eds., 1972, *Handbook of Mathematical Functions, with Formulas, Graphs, and Mathematical Tables* (New York: Dover), p. 504.

Bogdan, T. J., Cattaneo, F., and Malagoli, A. 1993, *Ap. J.* **407(1)**, 316.

Carrier, G. F., Krook, M., and Pearson, C. E. 1983, *Functions of a Complex Variable* (Ithaca, NY: Hod).

Dawson, T., and Fawcett, J. A. 1990, *J. Acoust. Soc. Am.* **87(3)**, 1110.

Goldreich, P., and Keeley, D. A. 1977, *Ap. J.* **212**, 243.

Goldreich, P., and Kumar, P. 1988, *Ap. J.* **326**, 462.

Goldreich, P., and Kumar, P. 1990, *Ap. J.* **363**, 694.

Goldreich, P., Murray, N., and Kumar, P. 1994, *Ap. J.* **424**, 466.

Gradshteyn, I .S., and Ryzhik, I. M. 1994, *Table of Integrals, Series, and Products* 5th Ed., ed. A. Jeffrey (Boston: Academic Press), p. 1063.

Libbrecht, K. G., and Woodard, M. F. 1991, *Science* **253**, 152.

Lighthill, M. J. 1952, *Proc. Roy. Soc. A* **211**, 564.

Lighthill, M. J. 1954, *Proc. Roy. Soc. A* **222**, 1.

Longuet-Higgins, M. S. 1989a, *J. Fluid Mech.* **201**, 525.

Longuet-Higgins, M. S. 1989b, *J. Fluid Mech.* **201**, 543.

Longuet-Higgins, M. S. 1990, *J. Fluid Mech.* **221**, 675.

Musielak, Z. E. 1987, *Ap. J.* **322**, 234.

Musielak, Z. E., Rosner, R., Stein, R. F., and Ulmschneider, P. 1994, *Ap. J.* **423**, 474.

Proudman, J. 1952, *Proc. Roy. Soc. A* **214**, 119.

Stein, R. F. 1967, *Solar Phys.* **2**, 385.

CHAPTER 3

A Simple Model of Plume Convection

Numerical studies of turbulent convection in a stratified atmosphere suggest that large scale, steady structures (plumes) play a significant role in the transport properties of the medium (Spruit, Nordlund and Title (1990), hereafter SNT; Stein and Nordlund (1989)). We develop a simple analytic model of axisymmetric plumes to provide insight into these calculations. In particular, we discuss the asymmetry between upward and downward directed flows, and develop an understanding of what sets the mixing length scale, commonly used in astrophysical calculations. The fibrillar downflows reported in the simulations are shown to be an artifact of poor resolution. For plumes with a fixed luminosity, we find that the scale of vertical mixing (the mixing length λ) depends very weakly on the Froude number ($\lambda \propto \mathcal{F}^{1/6}$). In addition, our calculations suggest that flows of this type undergo a 'phase' transition at some critical Froude number, $\mathcal{F}_c$, below which the flow takes the form of a plume, and above which the flow becomes a self-collimated jet.

The model differs in important ways from previous work describing plumes. In particular, it is argued that energy bearing upflows are of a sufficiently large scale that mixing on the horizontal boundary (entrainment) in not an important effect in determining its shape or transport properties. While we neglect entrainment as a mechanism for decelerating the flow, our model allows for a steady, subsonic pressure excess to develop at some height in the atmosphere. This is unavoidable if energy and mass are to be conserved simultaneously.

The pressure center brakes the rising vertical material and directs it outward. Most of the radial diversion occurs in a very thin layer, which gives the plume an anvil shape, as is commonly observed in convective structures in the Earth's atmosphere. For sufficiently low Froude numbers, there is always a well-defined top of the plume, with or without entrainment.

3.1 Introduction

The Mixing Length Theory (MLT) of turbulent convection has been widely applied in astrophysical problems. The theory has a long history of development, starting with the concurrent efforts of Schmidt, Taylor, and Prandtl,† (Schmidt(1941); Taylor (1945); Prandtl (1952)) and reaching canonical form in the work of Böhm-Vitense (1958). To the extent that MLT provides a reasonable estimate of the convective energy flux, it is sufficient to address a large number of problems in stellar structure and evolution. For the most part, numerical simulations of convection in gravitationally stratified atmospheres validate the mixing length concept (Chan and Sofia (1987)), but strongly suggest that the physical picture presented in MLT is flawed in important ways, and many features of the simulations cannot be readily interpreted within the framework of MLT (SNT). The purpose of this work is to present a model of turbulent plumes suitable for discussing the results of these simulations. The eventual goal is to adapt the Mixing Length Theory to accommodate a more physical view of the underlying processes involved in convection. To this end, several observations should be made to place our concerns in context.

The character of convective elements. Mixing length theory avoids a precise description of convective structures, and ignores any constraints imposed by the overall convective topology. The theory provides a physical picture of rising and sinking blobs of material, traveling with a single convective veloc-

† These authors essentially developed the same theory in parallel, although they disagree on some of the details. See Wasiutyński (1946) for an early review.

ity over a mixing length, and breaking up into smaller eddies for a variety of reasons. The connection between this picture and the apparent structures in 3-dimensional simulations is somewhat remote. Stratification distorts the buoyant eddy giving it an elongated shape. The essential structural component of a convecting atmosphere may be properly characterized as a turbulent plume (SNT), and a compelling theory of convection should be consistent with this observation. Moreover, without reference to the structures or topology of convection, MLT provides little insight into the problem of magnetic field transport, and a somewhat limited framework within which to discuss non-local effects, such as overshooting and undershooting.

The role of turbulent dissipation. The MLT makes implicit reference to the Kolmogoroff cascade as a mechanism for dissipation. The theory of homogeneous isotropic turbulence (HIT) has been applied to MLT, and convincingly argued to be relevant in several applications (Spiegel (1962); Goldreich and Keeley (1977ab)). However, the simulations suggest that this may be superfluous (SNT), since the topology of the flow does not allow for much interaction among eddies. Even for very large Reynolds numbers, the mean flow may be largely unaffected by turbulent mixing, which acts only to make the transport less efficient by diluting the buoyancy of the convecting material.

The determination of the mixing length. The choice of mixing length scale has long been a controversial subject (see Chan, Wolff and Sofia (1981) and the references therein). Uncertainty about the value of the mixing length parameter α remains the most unappealing feature of MLT. The intermittent nature of the convective flows directly conflicts with the idea of a fixed mixing length parameter, despite the fact that the mixing length hypothesis leads to mean entropy profiles consistent with simulations (Chan *et al.* (1981, 1982, 1984, 1986, 1987, 1989); Stein and Nordlund (1989)). By considering a theory based on plume transport, the mixing scale can be calculated explicitly and self-consistently, allowing for variation as a fundamental feature of the model.

The original theory of turbulent plumes is due to Morton, Taylor and Turner (1956), who studied systems in which buoyant material is ejected from small, point-like sources. The MTT theory was based partly on the work of Schmidt (1941) who viewed the observed conical plumes as a balance between horizontal turbulent diffusion of heat and momentum and vertical convection. Assuming the horizontal dependence of the fluid variables maintains a similar functional form along the plume, MMT derived a set of equations expressing the conservation of mass, vertical momentum and energy (buoyancy). In addition, the Boussinesq (1903) approximation and the entrainment hypothesis of Batchelor (1954) were integral parts of the theory. The latter assumption offers a way of reducing the complicated hydrodynamic phenomena to a simple statement: the infall velocity adding mass and cool material to the flow is proportional to the local vertical velocity. The constant of proportionality $\alpha \sim O(1/10)$ depends on the choice of horizontal profile. The assumption of horizontal similarity breaks down near the top of the plume where entrainment erases the density contrast. Although analytic modeling of convective plumes has received considerable attention in the meteorological and engineering literature, very few applications have been sought in astrophysical contexts, with certain notable exceptions (Moore (1967); Scalo and Ulrich (1973); Ulrich (1970abc); Schmitt, Rosner and Bohn (1984)).

While the MTT theory has been applied to the case of an extended source (through the use of virtual sources), large plumes with radial scales of order a density scaleheight present a new set of complications which must be addressed by a new model. Energy bearing upflows begin with a horizontal scale on this order and diverge upstream in order to conserve mass flux. The horizontal diffusion resulting from shear at the edge of the plume cannot fully mix the core, since the turbulence is advected away with the expanding flow. For this reason, entrainment in large scale plumes should be viewed as a surface effect which does not alter the transport along the central axis. Mixing is confined to a boundary layer which serves mainly to join the structure to the ambi-

ent medium. The mass, momentum and energy exchange at the *entrainment horizon* can be neglected to lowest order. On the other hand, for converging downflows, the antibuoyant material accelerates, producing large shears which quickly detrain and dissipate the flow.

The organization of the remainder of the chapter is a follows. In Section 3.2, the plume model is developed, and the implications of the model are discussed in Section 3.3. Section 3.4 discusses the limitations of the model and offers some suggestions for future applications, including an effort to construct a global theory of convection with the plume as the elemental structure.

3.2 The Plume Model

A plume is an isolated, steady (time-independent) flow structure superposed on the background atmosphere. For an upward-directed plume, the rising material carries excess heat relative to the ambient gas. The extra entropy in the region induces a buoyancy force causing the material to rise. Although the term plume connotes expansion, we also use it to describe downward-directed, convergent flows, driven by relatively cool material injected at the upper boundary. In either case, if the outer boundary conditions are time-independent, a steady structure will develop upstream, lasting as long as the source is maintained.

Since efficient convection leads to an adiabatically stratified atmosphere, we adopt a plane-parallel polytrope as a model for the ambient medium. For such an atmosphere occupying the region $z > 0$, hydrostatic equilibrium implies that $\rho_0 \propto z^m$, $p_0 \propto z^{m+1}$, $T_0 = gz/C_p$, and $s_0 = const.$, where ρ_0, p_0, T_0, and s_0 are the unperturbed density, pressure, temperature, and entropy, respectively. The constants g, C_p and m are the gravitational acceleration (assumed uniform), constant pressure specific heat and polytropic index. The gas has a constant Γ equation of state, with $\Gamma = 1 + 1/m$, and the density scaleheight at depth z is given by $H = z/m$. This background state is appropriate if the mean entropy deficit of the atmosphere is small compared to the entropy

contrast inside and outside the plume. Although neutral stability is assumed in the following derivation, one can easily extend our results to more general environments.

For sub-sonic convection, the ram pressure of the flow is small compared to the background pressure of the atmosphere (i.e., $\rho_0 v^2 \ll p_0 \sim \rho_0 c^2$, where c is the adiabatic sound speed). Our treatment allows for a pressure perturbation to develop on this order, as part of the hydrodynamic equilibrium. Most theories of sub-sonic convection, including all models of buoyant plumes, have neglected this based on the assumption that sound waves act quickly to erase any local variations which develop in the pressure. This assumption is questionable for several reasons. First, the high frequency sound waves are excited by forces *out* of equilibrium, only propagating when the net restoring force must be balanced by changes in inertia. A starting plume can develop quasi-statically, with gas pressure gradients balanced on the longer time scale by advection of momentum. Hence, the cancellation of pressure perturbations by sound waves occurs only to order $\delta p \sim \rho v^2$. Second, numerous meteorological structures with a net, sub-sonic pressure perturbation have been observed, all being formed on timescales long compared to the sound crossing time (e.g., hurricanes). Finally, the radial expansion of gas must be caused by *some* force with a component in that direction. This is required to escort the fluid aside and aid in conserving mass in the region of lower density upstream. Although earlier models of plumes omit the horizontal equation of motion, turbulent Reynolds stress is implicitly invoked as a source of horizontal momentum through the entrainment hypothesis, but this is not applicable to the large-scale, unmixed plumes. In order to incorporate the effect of gas pressure into our model, two additional equations must be included to govern the horizontal momentum and the perturbed pressure.

With the assumption of low Mach number ($M \equiv v/c \ll 1$) convection, it is appropriate to make approximations to the steady Navier-Stokes equa-

tions. Since pressure variations are quadratic in the perturbed fluid velocity, we retain the terms in the advective part of the fluid inertia, in contrast to approximations performed to derive linear wave equations. In the mean flow equations, for now, we neglect contributions from turbulent fluctuations which lead to mass and entropy entrainment. These effects are treated as a geometric correction below.

To develop a simple analytic model, we must assume a particular form of the cylindrical radial dependence of the perturbed variables. For point sources of buoyancy, two choices of profiles have been considered: a *top hat* model in which all the fluid variables are constant out to the horizontal plume boundary, and a *gaussian* model with one horizontal scale for the vertical velocity and another for the buoyancy (density and entropy contrast). Since both models lead to qualitatively similar equations, the choice is not critical, except when relating model parameters to experiment. The gaussian *ansatz* has been successfully applied to interpreting measurements of point source plume (Schmidt (1941), MTT). For problems in which the source region is extended, however, it is unlikely that small scale turbulence (which sets up the gaussian profile) will be available, so it may be inappropriate to extend the laboratory results to this case. Therefore, we adopt a quadratic profile to describe the flow *near the core of the plume*, and consider only the lowest non-vanishing terms in an expansion about $r = 0$. This procedure gives a simple set of equations whose interpretation is physically meaningful, and avoids altogether complications arising from profile modeling.

At any point along the central axis ($r \to 0$), the vertical velocity must approach a constant, and the pressure gradient must vanish. In addition, to obtain closure in the plume equations, we assume the radial motion is homologous to lowest order $v_r \propto r$, and any rotation is of solid body type.† Therefore,

† This is equivalent to stating that the physical variables are analytic to first order in their radial behavior. Notice that solid body rotation is consistent with

consider an *ansatz* of the form

$$\overline{\mathbf{v}} = -W(z)\hat{\mathbf{z}} + rU(z)/R(z)\hat{\mathbf{r}} + r\Omega(z)\hat{\phi} + \ldots, \tag{3.1}$$

for the mean velocity, and

$$\overline{\delta\rho} = \delta\rho_0(z)\left(1 - \left(\frac{r}{R(z)}\right)^2 + \ldots\right) \tag{3.2}$$

$$\overline{\delta p} = \delta p_0(z)\left(1 - \left(\frac{r}{R(z)}\right)^2 + \ldots\right) \tag{3.3}$$

$$\overline{\delta s} = \delta s_0(z)\left(1 - \left(\frac{r}{R(z)}\right)^2 + \ldots\right) \tag{3.4}$$

for the mean values of the perturbed density, pressure and entropy. The above *ansatz* is an expansion of the steady solutions to the Navier-Stokes equations for $r \lesssim R(z)$, where $R(z)$ is the radial scale over which the perturbed variables decay (the effective plume radius). One could take the above system as correct to all orders, except that its substitution into the Navier-Stokes equations implies that an additional scale (other than $R(z)$) is required to keep the system from being overdetermined. At the plume horizon, the core flow is joined by a turbulent boundary layer to the ambient medium.

The seven model functions include three velocity variables $\{W, U, \Omega\}$, three thermodynamic variables $\{\delta p_0, \delta\rho_0, \delta s_0\}$, and the plume radius R. Since there are only six relations among these functions generated by substituting (3.1) – (3.4) into the steady Navier-Stokes equations, closure requires an additional model relation for R. Notice that the outer plume radius is defined by

$$\frac{\overline{v}_r(R,z)}{\overline{v}_z(R,z)} = \frac{U}{-W} = \frac{\frac{dR}{dt}}{\frac{dz}{dt}} = \frac{dR}{dz}, \tag{3.5}$$

---

the homologous scaling, which can be seen by computing $d\Omega/dz$.

yielding the required relation

$$-W\frac{dR}{dz} = U \tag{3.6}$$

Manipulating the other six equations for the model variables, we obtain four first integrals (constants of the motion), a perturbed equation of state, and a first order ordinary differential equation for U

$$-W\frac{dU}{dz} = \frac{2Q}{R} + \Omega^2 R, \tag{3.7}$$

where the function $Q \equiv \delta p_0/\rho_0$ is the adiabatic part of the Eulerian enthalpy perturbation ($\delta H = Q + T\delta S$). Equation (3.7) is essentially the radial equation of motion with fluid inertia balanced by the pressure gradient and a possible centrifugal force.

The constants of the motion are the mass flux

$$\dot{M} = \rho_0 \pi R^2 W, \tag{3.8}$$

specific angular momentum

$$J = \Omega R^2, \tag{3.9}$$

entropy contrast

$$\epsilon = \frac{\delta s_0}{c_p}, \tag{3.10}$$

and the familiar Bernoulli constant

$$B = \frac{W^2}{2} + \Delta H, \tag{3.11}$$

where ΔH is the total enthalpy perturbation

$$\Delta H = Q + T_0 \delta s_0. \tag{3.12}$$

Noting that $T_0\delta s_0 = \epsilon g z$, the Bernoulli constant could also be considered to include the buoyancy potential as an effective external field. Since the model

describes the flow near the core of the plume, it is not surprising that the constant B appears to lowest order (it is a constant on the central axis streamline, which explains why there is no radial kinetic energy in this constant). Moreover, since B is the excess energy per unit mass carried by the flow, one can form an alternative constant, the luminosity of the plume

$$L = \dot{M}B = \rho_0 \pi R^2 W(W^2/2 + \Delta H), \tag{3.13}$$

which includes both kinetic and thermal contributions. If turbulent mixing is added to the model (in the form of entrainment term corrections), none of the integrals remain. In that case, mass, energy, and momentum are exchanged with the external medium, so none of these quantities is conserved.

Since only two thermodynamic variables are needed to specify a state, $\delta\rho_0$ does not appear in any of the above expressions. However, the density perturbation may be computed by

$$\delta\rho_0 = \rho_0 \left(\frac{Q}{c^2} - \epsilon \right) \tag{3.14}$$

once Q is known from the solution to the above equations. (3.14) is the perturbed equation of state.

Notice that the above model equations involve two distance scales - the scaleheight of the atmosphere and the plume radius. Hence, it is not possible from dimensional analysis to argue that the mixing length (the vertical scale for the plume which appears once the equations are integrated) should be proportional to the scaleheight. In fact, we shall see that the mixing length also depends on the ratio of the plume radius to scaleheight. However, if one measures the radius in units of local scaleheights, the above system is a *scale-independent* model of plumes. Thus, it describes plumes which originate at any point in the atmosphere, provided that the background remains adiabatically stratified.

To add the effect of entrainment to the model, we make the substitution $U \rightarrow U + \Delta U$, where ΔU is the expansion velocity of the boundary due to

turbulent diffusion (relative to the mean flow). According to the entrainment hypothesis, $\Delta U = \alpha W$, where α is the entrainment parameter. In Appendix **3.1**, we offer a justification of the constant α hypothesis. This extension of the basic model is only appropriate for fully mixed plumes, either small scale upflows or converging downdrafts. The effect of entrainment on global rotation is unclear at present, so we set $\Omega = 0$. Performing the substitution leads to the following set of equations for the remaining five independent variables:

$$\frac{dR}{dz} = -\frac{U}{W} - \alpha \tag{3.15}$$

$$-W\frac{dU}{dz} = \frac{2Q}{R} + \alpha\frac{UW}{R} \tag{3.16}$$

$$\frac{dB}{dz} = T_0\frac{d\delta s_0}{dz} \tag{3.17}$$

$$\frac{d\dot{M}}{dz} = \frac{2\alpha}{R}\dot{M} \tag{3.18}$$

$$C\frac{d\delta s_0}{dz} = (1-C)\frac{2\alpha}{R}\delta s_0. \tag{3.19}$$

The constant C depends on the assumed horizontal profile; for tophat and gaussian profiles, $C = 1/2$. The additional term in the horizontal momentum equation (3.16) is a model for the turbulent Reynolds stress. (3.17) implies that the energy carried by the flow is altered only by an exchange of heat with the atmosphere ($dB = T_0 d\delta s_0$), and equations (3.18), (3.19) model the entrainment of mass and buoyancy into the plume (they agree with the canonical plume models).

3.3 Implications of the Model

The system of ODE's (3.6), (3.7) are integrated from the source end of the plume in the direction of the initial vertical velocity, maintaining the constancy of the integrals (3.8) – (3.11). The solution depends only on the boundary conditions at the origin of the flow, which have the form of initial conditions at a depth $z = z_0$. To reduce the size of the solution parameter space, we

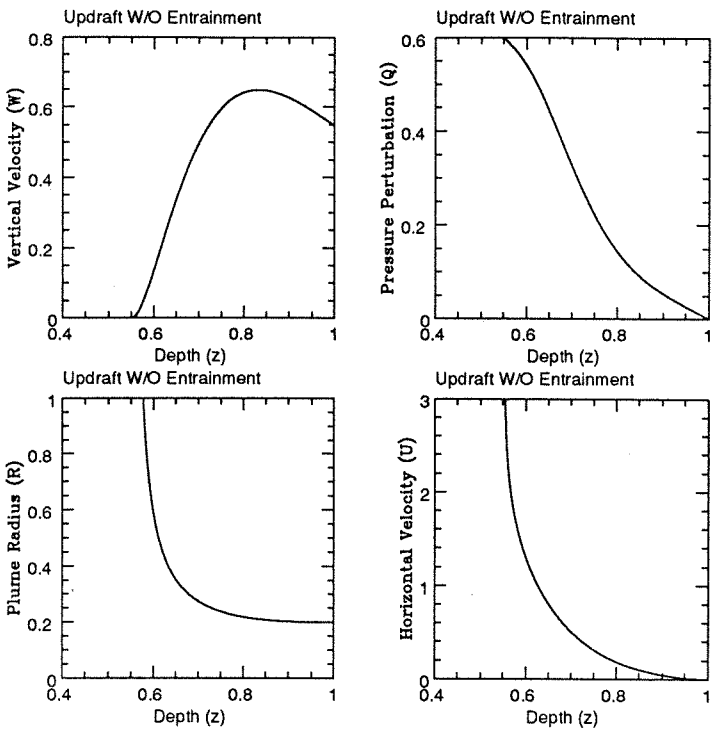

Figure 3.1: Sample Radius, Horizontal Velocity, Vertical Velocity, and Enthalpy Perturbation for Updrafts Without Entrainment. The equations were integrated with R/H=0.5 and $\mathcal{F}_0 = 0.15$. The singularity in radius occurs at $z \approx 0.554$. An entrainment parameter $\alpha = 0.1$ was used for all the calculations.

simplify our analysis to the case of no rotation ($\Omega = 0$), and require that the perturbed pressure and horizontal velocity vanish at the starting boundary. In that case the solutions to the zero entrainment model are scale-invariant and depend only on the dimensionless Froude number $\mathcal{F} \equiv W_0^2/\epsilon g z_0$ and the ratio of initial plume radius to the local density scaleheight $\beta \equiv R_0/H_0$.†

Figure 3.1 shows the behavior of the model variables for an upward-directed plume without entrainment. When entrainment is neglected, the updraft generically maintains a constant radius for most of the penetration distance, until suddenly the radius diverges. This divergence is caused by a

† Our definition of the $\mathcal{F}$ differs by a factor of R_0/z_0 from what is normally used in the literature. This makes comparison of the energy terms in equation (3.11) more convenient.

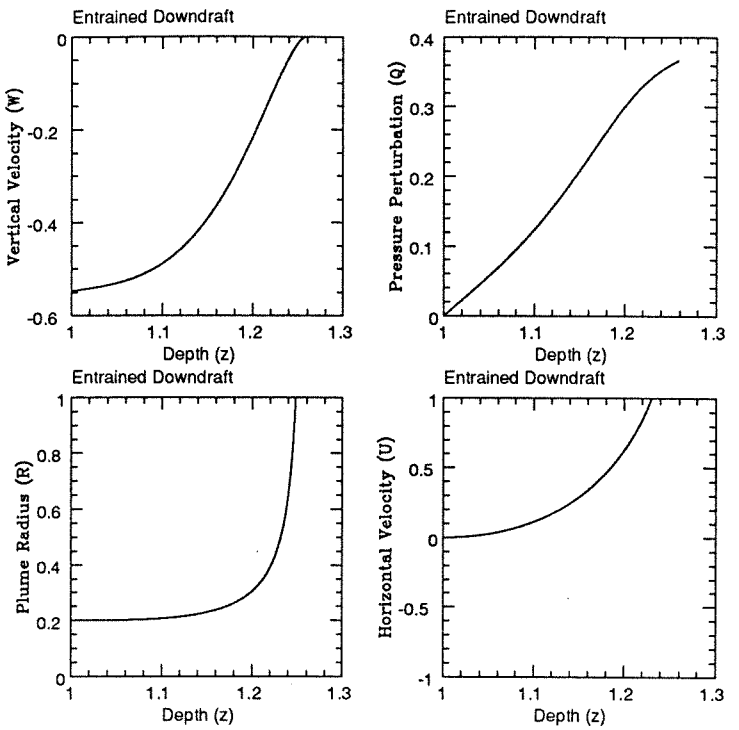

Figure 3.2: Sample Radius, Horizontal Velocity, Vertical Velocity, and Enthalpy Perturbation for Entrained Downdrafts. The equations were integrated with R/H=0.5 and $\mathcal{F}_0 = 0.15$. The downflow is also detrained by mixing.

mathematical singularity in the model equations, to which we devote a subsection below. When entrainment is included for the downdrafts, the plume diverges is the same fashion, as may be seen in Figures 3.2 and 3.3. Note the approximate conservation of the constants $\epsilon, \dot{M}, B$ and L.

The Figure 3.4 plots the dependence of the penetration scale on Froude number, for a fixed value of the initial plume radius (for updrafts without entrainment). The mixing scale λ depends on $\mathcal{F}$ as $\lambda \propto \mathcal{F}^{1/3}$, a scaling law that is justified in section 3.3.2.

Above some critical Froude number $\mathcal{F}_c$, the character of the flow shifts from a plume to a jet, although the strong shear in these solutions implies that the approximation used to derive the model equations has broken down. This shift is similar to a phase transition, because of the way the penetration scale λ approaches $\lambda_{\max}$ (the entire atmosphere). The singularity fits a power law of

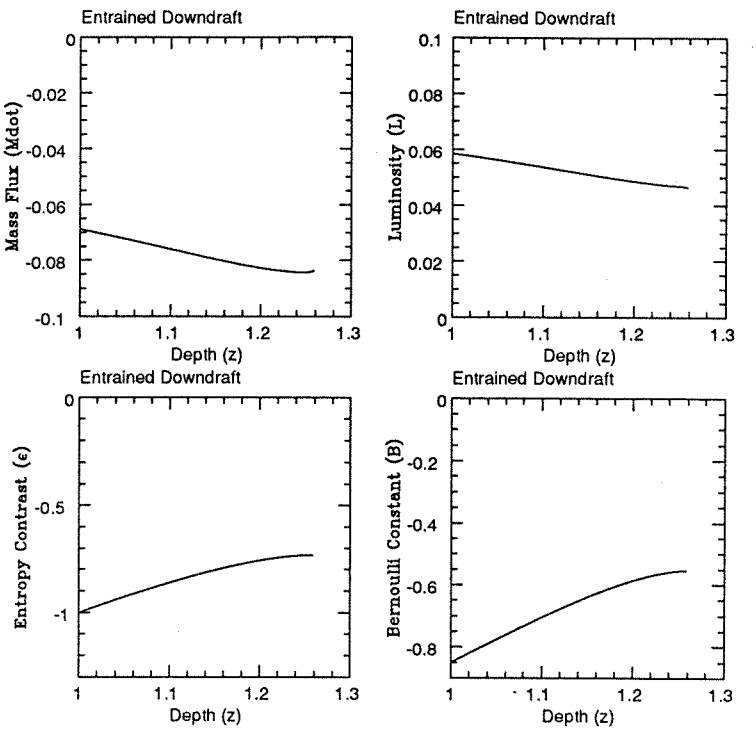

Figure 3.3: Sample Energy, Bernoulli Constant, Mass Flux, and Luminosity for Entrained Downdrafts. The equations were integrated with R/H=0.5 and $\mathcal{F}_0 = 0.15$. Note the approximate conservation of these quantities.

the form $\lambda_{\max} - \lambda \sim A|\mathcal{F} - \mathcal{F}_c|^\gamma$, with $\gamma \lesssim 1$. Typical values of $\mathcal{F}_c$ are of order 10 %, so we can confirm the assumption of the mixing length theory that the kinetic energy flux can be neglected when compared to the enthalpy term.

The next few subsections focus on some of the details of the qualitative results of this model.

3.3.1 Nature of the Anvil Singularity

The first equations of motion (3.6) can be written as

$$\frac{d}{dz}\left(\frac{1}{R}\right) = \frac{\rho_0 \pi U}{\dot{M}}, \tag{3.20}$$

using the mass flux constant. Integrating (3.20), one obtains a relation for the plume radius

$$R(z) = \frac{R_0}{1 - R_0 \int_z^{z_0} dz \frac{\rho_0 \pi U}{\dot{M}}}. \tag{3.21}$$

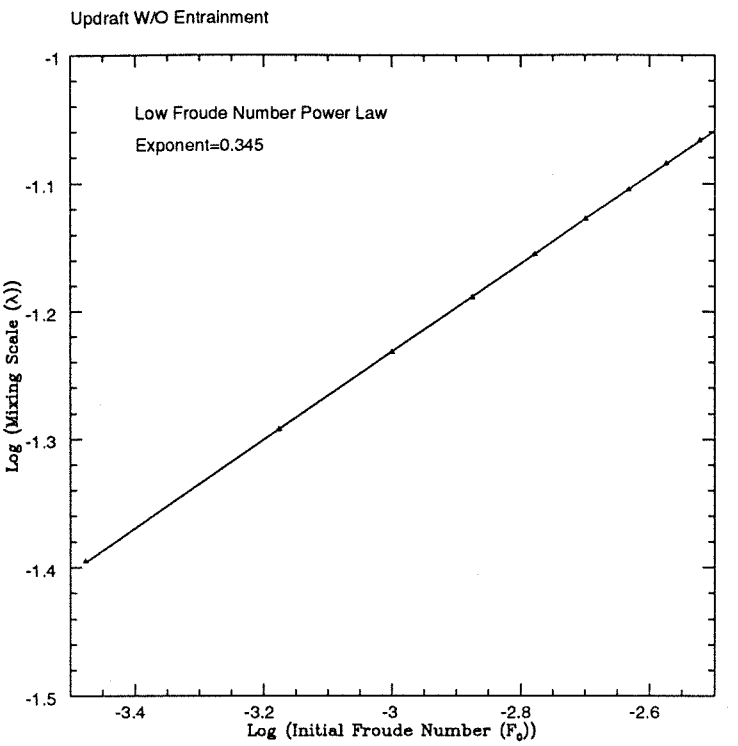

Figure 3.4: The Mixing Length as a Function of Froude Number for Upward-Directed Plumes. The best fit power law exponent was 0.345, close to the scaling law value of 1/3 discussed in the text.

Provided the plume is always expanding ($U > 0$), and rising $z < z_0$, there is a potential singularity in the plume equations at a height $z = z_c$ defined implicitly by

$$0 = 1 - R_0 \int_{z_c}^{z_0} dz \frac{\rho_0 \pi U}{\dot{M}}. \tag{3.22}$$

There is no guarantee that this condition will result from an arbitrary choice of initial conditions, but in practice it always occurs for plumes with sufficiently low Froude numbers. If the radius of the plume does diverge at some finite depth, it appears that the plume has an *effective* mixing length $\lambda = (z_0 - z_c)$. This can be computed by solving the plume equations.

To estimate the behavior of $R(z)$ as $z \to z_c$, consider the following argument. Near the critical depth z_c, the enthalpy perturbation approaches a constant $Q \to Q_c$. (That is, it changes much less rapidly than the diverg-

ing R or U). Making this approximation in (3.6),(3.7), the system has an approximate integral

$$U^2 \sim 4Q_c \log(R)\dagger. \tag{3.23}$$

Using this integral again in (3.20), one obtains an asymptotic relation

$$\frac{\sqrt{4Q_c}}{K_c}(z - z_c) \sim \int_R^\infty \frac{dR}{R^2\sqrt{\log R}} = \Gamma(1/2, \log R)$$

$$\sim \frac{1}{R\sqrt{\log R}}\left(1 + O\left(\frac{1}{\log R}\right)\right), \tag{3.24}$$

where $K_c = W_0 R_0^2 \rho_0/\rho_c$ is a constant and Γ is the incomplete Gamma function. Inverting the transcendental asymptotic relation to lowest order in $|z - z_c|$, one finds that the radius and horizontal velocity diverge as

$$R(z) \sim \frac{K_c}{\sqrt{4Q_c}} \frac{1}{z - z_c} \frac{1}{\sqrt{-\log(z - z_c)}}, \tag{3.25}$$

and

$$U(z) \sim 2\sqrt{Q_c}\sqrt{-\log(z - z_c)}. \tag{3.26}$$

The divergence of the plume radius is very nearly like a simple pole. However, while the factor $\sqrt{\log -(z - z_c)}$ is a slowly varying function, with higher order terms, it may give a substantial contribution to (3.25),(3.26). Combining the two expressions, another meaningful relation is

$$RU \sim \frac{\dot{M}}{\pi\rho_c(z - z_c)}. \tag{3.27}$$

Equation (3.27) can be used to show that mass is conserved as the plume spreads out. The horizontal mass flux is

$$\dot{M}_\perp = \int_{z_c}^{z} dz' \rho(z') 2\pi R(z') U(z') \frac{R(z)}{R(z')} \sim \dot{M}\left(1 + O\left(\frac{1}{\log(z - z_c)}\right)\right), \tag{3.28}$$

† Although the argument of the logarithm has dimension, bear in mind that this is an asymptotic relation. Any term involving a fiducial distance scale can be neglected in the asymptotic expansion, but may contribute corrections of order unity due to the weak divergence.

so the above divergence does not lead to contradictions with the conservation equations.

Inspection of the plume equations reveals that non-linearity is responsible for producing this singularity. Using the mass flux constant to rewrite the equation for U, one finds that both R and U increase unabated provided the pressure excess remains positive. In addition, the rate of increase in radius depends non-linearly on R and U. However, for sufficiently high Froude numbers, in order to conserve both mass and energy, the pressure perturbation must become negative, inducing an *infall* which continues to accelerate. In this case, a self-collimating jet appears, which is possibly destabilized by the sudden strong shear.

The above anvil singularity does not appear in models of plumes which neglect the pressure perturbation, and hence, has gone unnoticed in previous work. For those models, the flow is decelerated (or detrained) by dilution of the buoyancy when mass and lower entropy material is mixed at the plume horizon. Schmitt, Rosner and Bohn (1984) correctly point out an inadequacy of those models, that the material always remains buoyant (or anti-buoyant), and hence, it continues to accelerate without end. This problem is overcome by the inclusion of a pressure perturbation in the model. In addition, the model suggests that one need not invoke entrainment to regulate the accelerating flow; this naturally occurs by conservation of energy, mass and momentum.

Finally, we note that the anvil singularity occurs only if the flow is 3-dimensional. If one considers a 2-dimensional convective topology (a sheet source, as opposed to a bubble source), the resulting plume equations are identical to those above, with one exception. Mass conservation along the line now requires the mass flux per unit length

$$\dot{M}_L = \rho_0 W R \tag{3.29}$$

to be a constant. (In this case, R is the horizontal scale of the plume in the direction normal to the symmetry axis.) The above demonstration of the sin-

gularity is no longer valid. In fact, one can show that in 2-dimensional plumes, the vertical rise may be unbounded (see Appendix 3.2). This is interesting because the cylindrical flows may be unstable and take on a 2-dimensional shape. Moreover, it is noted several times in the simulations (see Stein and Nordlund (1989)) that the convection 'cells' appear sheetlike.

3.3.2 Scaling Relations for The Mixing Length Parameter

The dependence of the mixing length on the initial plume radius R_0 and Froude number $\mathcal{F}$ can be determined from the following argument. The singularity in the system (3.6),(3.7) appears when $\Delta R \sim R$ and $\Delta U \sim U$, while the vertical velocity $W \to 0$. At that point, for very low Froude numbers $\mathcal{F} \ll 1$, conservation of energy forces the enthalpy perturbation to behave like $Q \sim \epsilon g(z_0 - z)$ (only these two terms survive in the Bernoulli constant as $W \to 0$). Setting the mixing length $\lambda \sim (z_0 - z_c)$ in the ODE's (3.6),(3.7) gives a scaling relation

$$\lambda^3 \sim R_0^2 z_0 \mathcal{F}. \tag{3.30}$$

In terms of the local density scaleheight, the mixing length parameter behaves like

$$\alpha \sim \mathcal{F}^{1/3} \left(\frac{R_0}{H_0}\right)^{2/3}, \tag{3.31}$$

when $\mathcal{F} \ll 1$.† For modest Froude numbers up to the critical value $\mathcal{F} \lesssim \mathcal{F}_c \lesssim 1$, the enthalpy excess driving the horizontal flow approaches the Bernoulli constant, which implies a scaling relation

$$\lambda \sim R_0 \mathcal{F}^{1/2}. \tag{3.32}$$

In either case, the mixing length is not simply proportional to the scaleheight; it depends on the initial horizontal scale of the flow, as well as the Froude number.

---

† Unfortunately, α is used for both the entrainment function and the mixing length parameter. This hints at the fact that the two fields have not been joined.

The luminosity of the plume scales as

$$L \propto \left(\frac{R_0}{H_0}\right)^2 \mathcal{F}^{1/2}(1+\mathcal{F}). \tag{3.33}$$

For plumes carrying a fixed luminosity, with low $\mathcal{F}$, $R_0 \propto H_0 \mathcal{F}^{-1/4}$. Hence, energetically important plumes mix on a scale

$$\lambda \propto \mathcal{F}^{1/6}, \tag{3.34}$$

for low Froude numbers. One infers that the mixing length is very weakly dependent on the initial conditions which gave rise to the plume. Moreover, expressing (3.34) in terms of the plume radius, one has

$$\lambda \propto \left(\frac{R_0}{H_0}\right)^{-2/3}, \tag{3.35}$$

at fixed luminosity. In the absence of entrainment, smaller plumes would transport energy over a longer path. When entrainment is included, only the larger plumes with $R_0 \sim H_0$ are not detrained by turbulent mixing. On the other hand, if the plume gets too large, the constant luminosity mixing length decreases, making the transport process less efficient. A compromise between these two effects is reached when the plume radius is of order a local scale-height. Since the model is scale invariant, this statement is true of all plumes, regardless of their points of origin in the atmosphere. For Froude numbers approaching criticality, these arguments remain valid, although the scaling exponents differ.

3.3.3 The Downflow/Upflow Asymmetry

Many authors have noted the asymmetry between downflows and upflows in a stratified atmosphere (see Stein and Nordlund (1989)). The simulations suggest a characterization of downflows as fibrillar, spiraling and convergent, often penetrating through many scaleheights of atmosphere. When entrainment of mass into the downdraft is allowed, the structure quickly dissipates and loses coherence. The result of the simulations appears to be caused by a lack of resolution, since the flow converges to a scale for which the Reynolds number of the code is too small to simulate entrainment correctly.

3.4 Discussion

The utility of the plume as a meaningful elemental flow requires several assumptions. The source must be maintained for more than one rise time, the flow must not cause other motions which disturb the source, and the structure must be stable. In order to sustain the structure, it must be fed with heated gas at its lower boundary, which depends on the environment in which the plume resides. Plume lifetime and stability are the subject of a future investigation. One of the unfortunate features of the model is that the rise time $\tau \equiv \int_{z_c}^{z_0} \frac{dz}{v_z}$ formally diverges, although it is clear that the model breaks down when the singularity is approached.

Petrovay (1990) has offered a generalization of MLT which should be mentioned by way of comparison. Two topological types (ascending and descending flows) and two filling factor classes (cellular and fibrillar) are identified in the simulations, leading to four morphological categories. Making plausible assumptions about the statistical distributions of horizontal and vertical velocities, Petrovay forms a closed set of equations from which the filling factors can be calculated. The model is used to obtain a basic understanding of the overall topology of convection, and its use would be more compelling if the distribution function could be understood better.

In future work, we plan to develop a global theory of convection in which the atmosphere contains an ensemble of independent plumes. Schmidt, Rosner and Bohn (1984) have suggested one way to form a closed set of stellar structure equations using a plume model, as have Scalo and Ulrich (1973). We anticipate making only minor refinements to make our model suitable for applications. Since the behavior of the solutions is scale invariant, we envision the convecting environment consisting of a network of nested plumes, with smaller plumes high in the atmosphere fed by the heat transported by the larger structures below.

The ideas presented in this chapter should also have some bearing on the theory of the excitation of the solar p-modes, as well as the transport of magnetic fields through the solar convection zone. A more physical picture of convection may provide insight into the detailed modeling of acoustic wave generation. Moreover, an appreciation for the topological properties of the flow is required to understand the redistribution of fluxtubes, which is at the heart of the dynamo problem.

Appendix 3.1

An Alternative Derivation of the Entrainment Function

The entrainment hypothesis of Taylor (1945) holds that the infall velocity at the boundary of a turbulent buoyant plume is proportional to the vertical velocity along the central axis. The 'constant' of proportionality, α, is known as the entrainment function. Several forms of the function have been proposed (Schatzmann (1978), Schmitt *et al.* (1984)), although a constant entrainment function is adequate for our purposes.

Consider a turbulent flow which is steady ($\partial_t = 0$) and axisymmetric ($\partial_\phi = 0$) in the mean field. Within the Boussinesq (1903) approximation, the continuity equation becomes

$$\nabla \cdot (\rho_0 \overline{\mathbf{v}}) = 0. \qquad (A3.1.1)$$

Hence, there exist well-defined streamlines for the mean flow, with stream function, M:

$$\overline{v}_z = \frac{1}{\rho_0}\frac{1}{r}\frac{\partial r M}{\partial r} \qquad (A3.1.2a)$$

$$\overline{v}_r = -\frac{1}{\rho_0}\frac{\partial M}{\partial z}. \qquad (A3.1.2b)$$

Notice that $(A3.1.1)$ is linear in $\overline{\mathbf{v}}$, so the mass flowing between any two stream surfaces is conserved within this approximation. To say that the plume 'entrains' mass is to say that the plume radius does not coincide with a streamline. For an arbitrary function $R(z)$, one has an identity

$$\frac{d}{dz}\left[\rho_0(z)\int_0^{R(z)} dr 2\pi r \overline{v}_z(r,z)\right] = 2\pi R \rho_0 \left\{\frac{dR}{dz}\overline{v}_z(R,z) - \overline{v}_r(R,z)\right\}. \qquad (A3.1.3)$$

Define the *entrainment velocity* as

$$v_e(z) \equiv \frac{dR}{dz}\overline{v}_z(R,z) - \overline{v}_r(R,z). \qquad (A3.1.4)$$

v_e is the infall velocity at the boundary. One is free to define R in any manner. However, if self-similarity of the radial profile is to remain valid, a particular

definition may be required. If W is the area-averaged vertical velocity, then the entrainment function is given by

$$\alpha = v_e(z)/\overline{v}_z(0,z). \qquad (A3.1.5)$$

Moreover, the plume radius obeys the equation

$$\frac{dR}{dz} = \frac{\overline{v}_R(R,z)}{\overline{v}_z(R,z)} + \alpha\frac{\overline{v}_z(0,z)}{\overline{v}_z(R,z)}. \qquad (A3.1.6)$$

The assumption that W scales with the central and outer vertical velocities then justifies the model equation (3.15) up to a sign convention.

As an alternative, consider a plume radius defined implicitly by the relation

$$\overline{\delta S}(R(z),z) = \eta\overline{\delta S}(0,z), \qquad (A3.1.6)$$

where $\eta \lesssim O(1)$ is a constant. This equates the plume radius with the surface on which the entropy excess is a fixed fraction of the value on the central axis. Then the energy equation implies

$$\frac{dR}{dz} = \frac{\overline{v}_R(R,z)}{\overline{v}_z(R,z)} - \frac{\overline{\mathbf{v}}\cdot\nabla\overline{\delta S}(R,z)}{\overline{v}_z(R,z)\frac{\partial\overline{\delta S}}{\partial R}(R,z)} + \frac{\frac{\partial \ln|\overline{\delta S}(0,z)|}{\partial z}}{\frac{\partial \ln|\overline{\delta S}(0,z)|}{\partial r}}. \qquad (A3.1.7)$$

The later two terms are approximately constant if the eddy diffusion coefficient scales like $\mathcal{D} \sim R\overline{v}_z$.

Appendix 3.2

Two-Dimensional Plumes

The possibility of 2-dimensional (sheet-like) plumes is sufficiently great to warrant some consideration (SNT)). In this case, constancy of the mass flux along the sheet ($\dot{M}_L = \rho_0 WR = const.$) allows the equation for the horizontal plume scale to be written

$$\frac{d\ln(R)}{dz} = -\frac{\rho_0 U}{\dot{M}_L}. \qquad (A3.2.1)$$

This equation has exponential solutions

$$R(z) = R(z_0)\exp\{\int_z^{z_0} dz\rho_0 U/(\dot{M}_L)\}, \qquad (A3.2.2)$$

which need not possess singularities as in the 3-dimensional case. This does not appear to be a problem, because the power law divergence resumes in $2+\epsilon$ dimensions.

Chapter 3 References

Batchelor, G. K. 1954, *Quart. J. R. Met. Soc.* **80**, 339.

Böhm-Vitense, E. 1958, *Z. Ap.* **46**, 108.

Boussinesq, J. 1903, *Théorie Analytique de la Chaleur*, Vol. 2 (Paris: Gauthier-Villars), p. 172.

Chan, K. L., Sofia, S., and Wolff, C. L. 1982, *Ap. J.* **263**, 935.

Chan, K. L., and Sofia, S. 1984, *Ap. J.* **282**, 550.

Chan, K. L., and Sofia, S. 1986, *Ap. J.* **307**, 222.

Chan, K. L., and Sofia, S. 1987, *Science* **235**, 465.

Chan, K. L., and Sofia, S. 1989, *Ap. J.* **336**, 1022.

Chan, K. L., Wolff, C. L., and Sofia, S. 1981, *Ap. J.* **244**, 582.

Goldreich, P., and Keeley, D. A. 1977a, *Ap. J.* **211**, 934.

Goldreich, P., and Keeley, D. A. 1977b, *Ap. J.* **212**, 243.

Moore, D. W. 1967, in *Aerodynamic Phenomena in Stellar Atmospheres*, ed. R. N. Thomas (New York: Academic Press), p. 405.

Morton, B. R., Taylor, G. I., and Turner, J. S. 1956, *Proc. Roy. Soc. A* **234**, 1.

Petrovay, K. G. 1990, *Ap. J.* **362**, 722.

Prandtl, L. 1952, *Essentials of Fluid Dynamics* (London: Blakie).

Scalo, J. M., and Ulrich, R. K. 1973, *Ap. J.* **183**, 151.

Schatzmann, M. 1978, *Atmospheric Environment* **13**, 721.

Schmidt, W. 1941, *Z. Angew. Math. Mech.* **21**, 265.

Schmitt, J. H. M. M., Rosner, R., and Bohn, H. U. 1984, *Ap. J.* **282**, 316.

Spiegel, E. A. 1962, *J. Geophys. Res.* **67**, 3063.

Spruit, H. C., Nordlund, Å., and Title, A. M. 1990, *Annu. Rev. Astr. Astrophys.* **28**, 263.

Stein, R. F., and Nordlund, Å. 1989, *Ap. J.* **342**, L95.

Taylor, G. I. 1945, *Dynamics of a Mass of Hot Gas Rising in Air (US AEC MDDC 919, LDAC 276).*

Ulrich, R. K. 1970a, *Astrophy. Space Sci.* **7**, 7.

Ulrich, R. K. 1970b, *Astrophy. Space Sci.* **7**, 183.

Ulrich, R. K. 1970c, *Astrophy. Sp. Sci.* **9**, 80.

Wasiutyński, J. 1946, *Astrophysica Norvegica* 4, 13.

CHAPTER 4

Observations of High Degree Solar p-Modes

High resolution observations of the solar p-modes ($\ell \lesssim 2000$) are presented, with measurements of the dispersion relation and estimates of the mode amplitudes. The data set consists of a 4 hour time series of disk-centered Doppler images taken under good seeing conditions with a 7700 $\AA$ Cacciani Cell magneto-optical filter at Big Bear Solar Observatory. The mode energy distributions inferred from the data fit the Boltzmann (exponential) form extremely well, offering evidence in support of the stochastic excitation model.

4.1 Introduction

The solar oscillations of high spherical harmonic degree ($\ell \gtrsim 100$) have been observed by various groups in recent years (Tarbell *et al.* (1988); Libbrecht and Kaufman (1988); Tomczyk (1988); Dolfuss (1990); Kaufman (1991); Rhodes *et al.* (1991); Fernandes (1992); Fernandes *et al.* (1992)), but important questions remain unanswered. Accurate estimates of the mode energies and lifetimes (coherence times) are still unavailable for this range of horizontal wavenumbers, although reliable frequency measurements exist. The difficulty with obtaining quality measurements of mode energies is due to the degradation of spectral power on short scales from atmospheric seeing, and the determination of coherence times requires high quality observations of duration longer than the predicted lifetimes, of order days to weeks. The decline in power can be extreme, by a factor of as much as two decades.

Since the eigenfunctions of the highest horizontal wavenumbers are lo-

calized in the top layers of the sun, further study of these modes is required to probe this important region. Existing solar models are most uncertain in the few scale-heights beneath the photosphere, due to our incomplete understanding of compressible convection and order unity Mach number turbulence. Moreover, according to the prevailing model for the excitation and damping of the p-modes (Goldreich and Kumar (1990,1991); Goldreich, Murray and Kumar (1994); Goldreich and Murray (1994)), strong turbulence in the upper convection zone generates, absorbs and scatters the waves. Hence, improvements in observation in this regime are critical to test predictions of the theory.

In this chapter, we analyze a time series of velocity images (Dopplergrams) taken with a magneto-optical filter mounted on the 10 in refracting telescope at Big Bear Solar Observatory (BBSO).† The filter was the 7700 $\AA$ (Potassium) Cacciani Cell described by Cacciani (1993). Aside from providing estimates of the mode frequencies and amplitudes, our observations offer a suitable test for the stochastic excitation model of Goldreich *et al.* (1994). The model makes specific predictions regarding the dependence of mode energy on frequency and wavenumber. The theory holds that modes with frequencies at the peak of excitation ($\nu \sim 3.3$ mHz) are in 'thermodynamic equilibrium' with the convective eddies in the exciting region below the photosphere, and all should have the same energy according to equipartition. The low n p-modes and f-mode should depart from this standard, however, since these are nearly incompressible are more difficult to excite. (See Chapter 2 and Goldreich *et al.* (1994) for an anticipation of this effect.) In fact, such a decline in peak mode power is found in our data, particularly for the f-mode. Moreover, the instantaneous mode energy distributions inferred from the data follow a Boltzmann profile, in agreement with the theory.

The observation was partly motivated to test certain results reported in a

† A video of these observations is available from BBSO by reference to the observation date.

thesis by Kaufman (1991). To some extent, the work described in this Chapter is a reproduction of the main part of that thesis. For that reason, much of our technique is based on Kaufman's work. The main difference between the two observations is that Kaufman used a Lyot filter, and a Cacciani Cell was used to obtain our data. For the most part, the latter filter results in images of better quality. There are also several instances in which different approaches to data reduction and analysis were taken, and these are noted below. (Refer to Kaufman (1991) for a detailed discussion of the observational technique.)

The remainder of the chapter is structured as follows. In section 4.2, the data set and observational parameters are described. Section 4.3 discusses the reduction and analysis performed on the data. The final section discusses the implications of our observations and compares the results to previous work.

4.2 Description of Data Set

The Data Set consists of a sequence of velocity images taken at the center of the solar disk. The sampling was done at a rate of one image per minute, yielding a Nyquist frequency of 8.333 mHz. Our goal was to obtain a time series of duration several hours under good seeing conditions. Over the course of a two week observation run, only one sequence of high quality data resulted. In addition to the Doppler data, every 15 minutes the telescope was pointed to the limb where a white light image was taken to measure the Modulation Transfer Function (MTF). (See section 4.3.2 for a discussion.) Table 4.1 outlines the parameters of the observation.

Calibration measurements were performed before and after the time series, since the telescope was busy in the interim period. The dimensions of the field of view were determined by fixing the telescope on a small sunspot, moving a known angular distance, and measuring the displacement of the spot center in pixels corresponding to that angle. The full field of view was determined to be $304'' \times 228''$ or 224Mm $\times$ 168Mm. The average velocity signal was measured at two locations along the solar equator and related to a physical velocity by

comparison with the known solar rotation, after correcting for the motion of the Earth.

Although the observation continued for 7 hours, only the first 4 hours were selected for reduction. This first segment offered an uninterrupted series of uniformly good seeing, while the latter period had several gaps in the data and a general decline in image quality. The increase in observation time would only improve the frequency resolution by a factor of two, and the benefit is offset by image gap error and loss of coherence in the highest wavenumber modes. Moreover, it is unlikely that the observed mode linewidths are related to the actual lifetimes, expected to be of order several days.

Table 4.1

Observational Parameters

Date	1991 August 9
Time (UT)	16:30–20:30
No. of Images	240
Telescope	BBSO 10 in Refractor
Image Size	$304'' \times 228''$
Number of Pixels	497×473
Horizontal Image Scale	$0.593''$/pixel
$R_\odot$	$948''$
K-Space Scale Factor, $d\ell/dk$	21.38
Qualitative Seeing	GOOD

4.3 Data Reduction and Analysis

Reduction and analysis of the data involved several steps briefly outlined in the subsections that follow.

4.3.1 Fourier Analysis of the Data

The calibrated signal in the Dopplergrams gave a digitized surface velocity map $v(x, y, t)$. (Figure 4.1 shows a typical Dopplergram.) After trimming the noisy pixels from the edge of the image, the Fourier components $\tilde{v}(k_x, k_y, t)$ for the plane-parallel projected horizontal wavefunction were computed using the standard FFT algorithm with a Welsh window. (See Press *et al.* (1992) for a description of the numerical procedure.) The wavevector magnitude $k = |\mathrm{k}|$ is related to the spherical harmonic degree l by the scale factor dl/dk in Table 4.1. For each k, a temporal FFT was performed on the time series $\tilde{v}(k_x, k_y, t)$ resulting in positive and negative frequency spectral components $\tilde{v}(k_x, k_y, \omega)$ with a frequency resolution 69.4μHz. The velocity power peaks at certain frequencies corresponding to the different radial node numbers, n. Spikes in the power spectra appear like 'emission lines' in an electro-magnetic spectrum. Finally, the surface velocities of the modes, $v_\odot(\mathrm{k}, n)$, were computed by doing a multi-gaussian ridge fit of the power spectra. (See Libbrecht and Kaufman (1988) for a discussion of the ridge fitting algorithm.) A contour plot of the Spectral Power is given in Figure 4.2, and Figure 4.3 shows the power spectra for various values of ℓ.

The use of the term *mode* to describe the observed waves is somewhat misleading. The horizontal modes occur because of the periodic boundary condition on the sphere, which is not applicable to our limited field of view. Moreover, resolution in wavenumber is limited by the image scale, and each Fourier component k corresponds to $d\ell/dk \sim 20$ global modes. For this reason, groups of modes (wave packets) were observed, rather than quantized, global modes. Traveling at the group velocity $v_g = \partial\omega/\partial k \approx \omega/2k$, any wave train has a transit time across the image of a few hours at most. Hence, these are

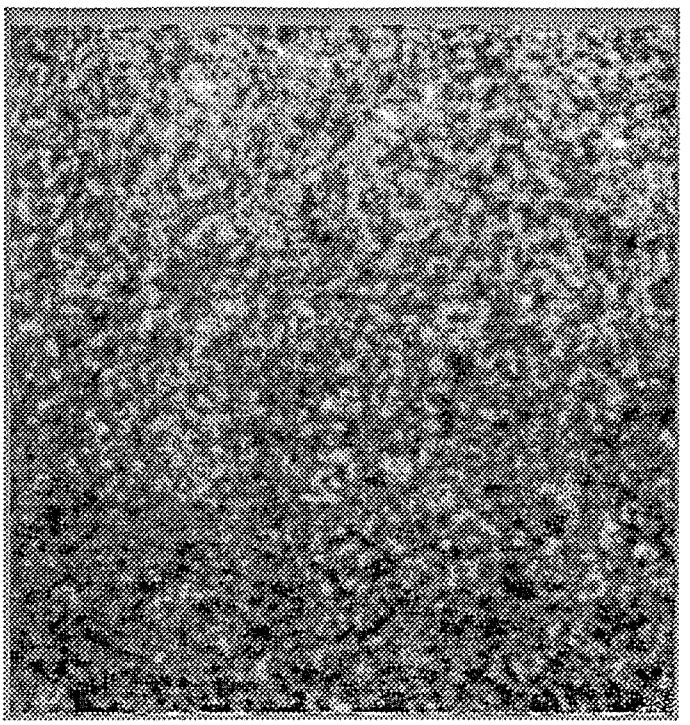

Figure 4.1: A Typical Doppler Image. The high quality of the data is seen in this image. The top of the graph is the eastern direction; one can see a trend in the signal from light to dark which results from the line-of-sight solar rotation.

observations of traveling disturbances, not modes. A future study of these wave packets using wavelet analysis could prove interesting in this regard.

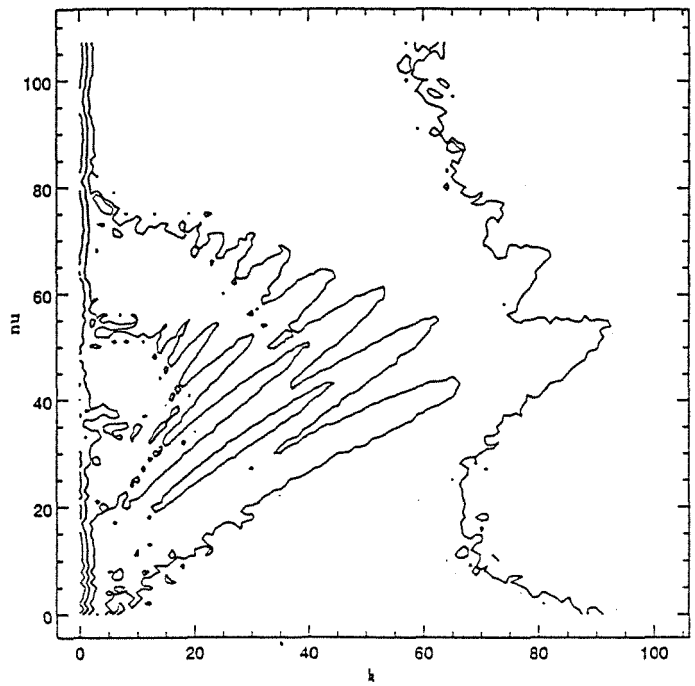

Figure 4.2: Contour Plot of Power Spectra. The uncorrected power is shown, and the axes are the integer indices from the Fourier transform grid.

4.3.2 Mode Frequency and Energy Measurements

The mode frequencies were taken from the ridge fits described in the previous section. A plot of the dispersion relation for the observed waves (an $\omega - k$ diagram) is found in Figure 4.4. The ridge structure is apparent up to order $\ell \sim 2000$. Dark triangles are from this data, horizontal lines from Kaufman (1991), and the theoretical eigenfrequencies of Kumar (1988) (using the solar model of Christensen-Dalsgaard (1982)) are shown in fine points. The lowest ridge corresponds to the nodeless ($n = 0$) f-mode, the incompressible surface gravity wave with theoretical dispersion relation $\omega^2 = gk$. There is good agreement with theory for our observed f-mode frequencies, which depart from Kaufman's (1991) reported negative frequency shift of order 10s to 100s of μHz. On the other hand, our p-mode frequencies agree more with Kaufman, showing a trend which is consistently lower in value than predicted by the model. The k-space scale factor was adjusted to match the measured low-ℓ frequencies, and

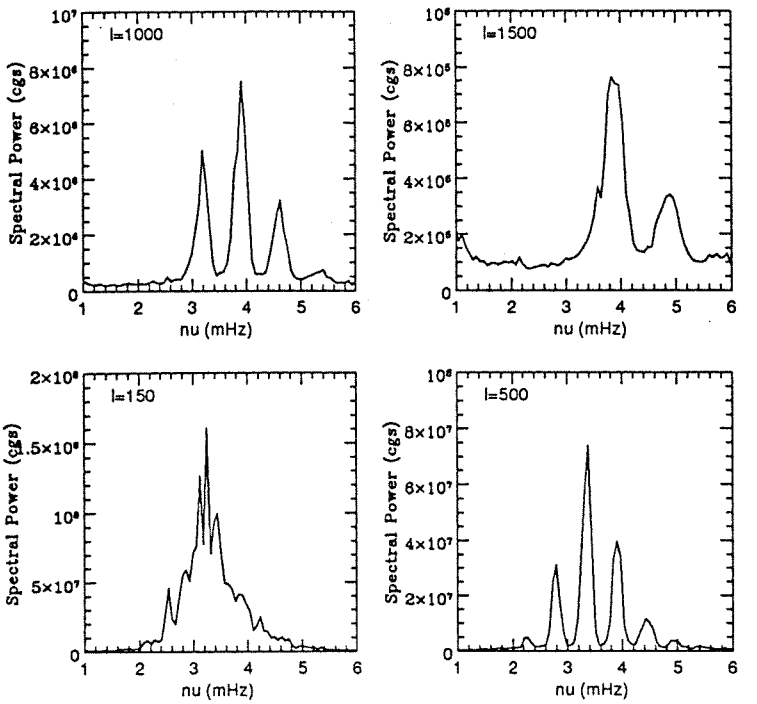

Figure 4.3: Selected Power Spectra. The peaks correspond to the different values of n for the fixed wavenumber.

this corrects for the systematic frequency shift due to background power with gaussian ridge fits (see Kaufman (1991)).

The mode energies are related to the surface velocity through the mode mass, $M(\ell, n)$, as $E(\ell, n) = M(\ell, n)v_{\odot}^2(\ell, n)$. Once again, the eigenfunction solver of Kumar (1988) was used to determine the mode masses. Figure 4.5 shows the inferred mode energies on a logarithmic scale, as a function of l for each of the 8 ridges seen in the data (n=0,1,...,7). Figure 4.6 plots the mode energies with a correction for the seeing degradation (the Modulation Transfer Function). (The next section describes this correction.) Finally, peak energy per mode is shown as a function of degree in Figure 4.7. There is an apparent decline in mode energy with increasing ℓ even with a seeing correction.

4.3.3 The Inferred Modulation Transfer Function

The degradation of velocity images due to atmospheric seeing was corrected in the spatial spectra using a technique developed by Kaufman (1991).

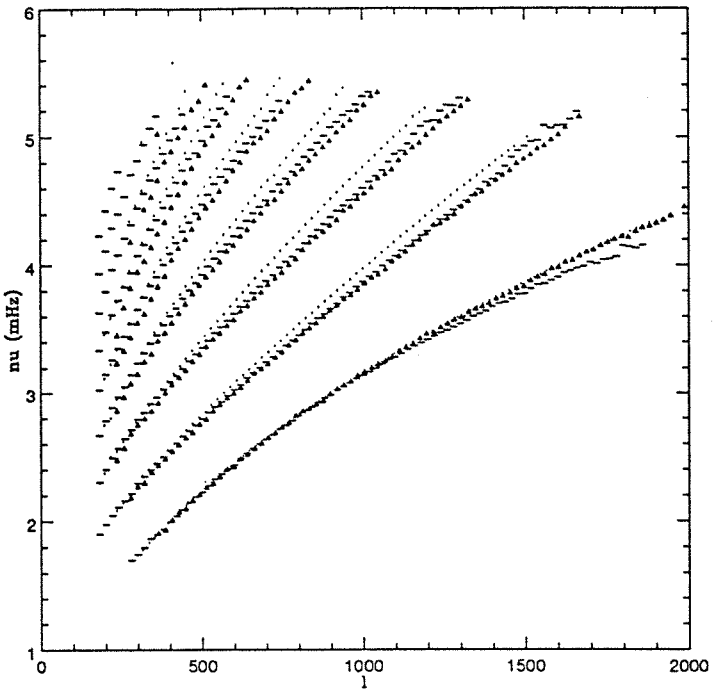

Figure 4.4: The Measured Dispersion Relation. The dark triangles are this data, the horizontal lines from Kaufman's 1987 data (1991), and the theoretical frequencies are shown in fine points.

The smearing of light on the limb of the sun offers a quantitative estimate of the Point Spread Function (PSF). This was determined by inverting the distributed light profile with respect to a theoretical limb intensity function. The MFT is then found as the FFT of the PSF. A simple gaussian PSF with a FWHM of 1″ was used to correct the data, and this was consistent with the limb smearing scale. The correction for power degradation is largely uniform in time, so a single MTF was used. This differs from the technique of Kaufman (1991), who corrected the spatial spectra before performing the temporal FFT. At several arcseconds of scale, the MTF is down by a factor of order 10, so the correction is quite large. The tail of the MTF is quite uncertain in this region as well, due to its sensitivity on the limb light profile model. For this reason, more elaborate modeling of the MTF lacks justification.

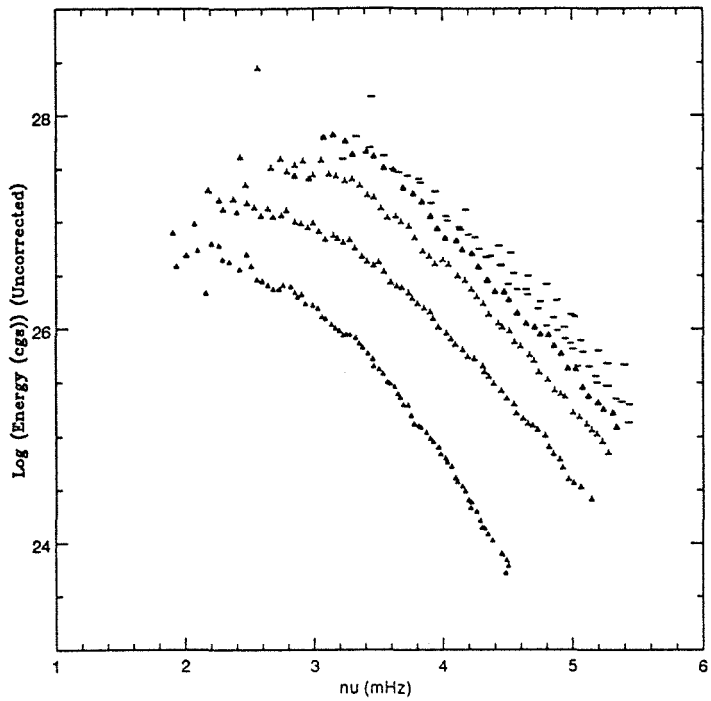

Figure 4.5: The Measured Mode Energies as a Function of Frequency. The different ridges are marked as follows: dark triangles for the f-mode ($n = 0$), bold skeleton triangles for p_1 ($n = 1$), light skeleton triangles for p_2 ($n = 2$), open triangles for p_3 ($n = 3$), and horizontal lines for $p_4 - p_7$ ($n = 4, 5, 6, 7$). Note the decline in mode energy with decreasing n (increasing l) at fixed frequency.

4.3.4 The Inferred Instantaneous Energy Distribution

The stochastic excitation model predicts that the observed mode energies should follow a Boltzmann (exponential) distribution (Kumar, Franklin and Goldreich (1988); Gabriel (1993ab)). In Appendix 4.1, we give an independent account of this result, showing that this distribution is a stationary solution to the Fokker-Planck equation for the state distribution of a damped harmonic oscillator driven by White Noise.

The spatial Fourier amplitudes, $|\tilde{v}(\mathrm{k}, t)|^2$, were used as proxy for the mode energies at fixed k. For sufficiently high wavenumbers, only the f-Mode is substantially excited ($\ell \gtrsim 1500$). Fixing k and the radial node number n, all the modes should the same mass and reduction in amplitude from seeing. (The

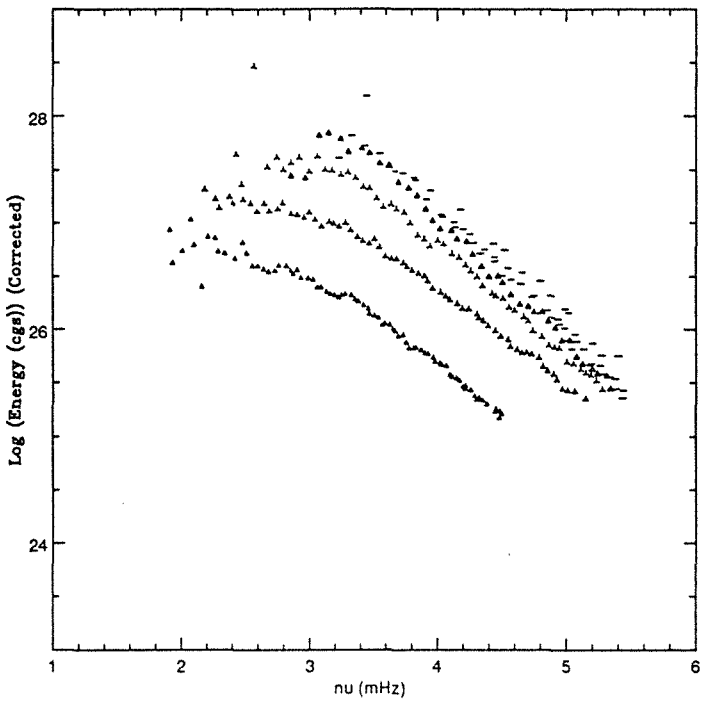

Figure 4.6: The Measured Mode Energies as a Function of Frequency (Corrected). The different ridges are marked as follows: dark triangles for the f-mode ($n = 0$), bold skeleton triangles for p_1 ($n = 1$), light skeleton triangles for p_2 ($n = 2$), open triangles for p_3 ($n = 3$), and horizontal lines for $p_4 - p_7$ ($n = 4, 5, 6, 7$). Note the decline in mode energy with decreasing n (increasing l) at fixed frequency still exists when a correction is made for loss of power due to seeing.

MTF is assumed to be a function of k only.) Hence, up to a constant change of scale along the ordinate, at each time slice, the distribution of $|\tilde{v}(\mathbf{k}, t)|^2$ resembles that of the instantaneous distribution of mode energies. The data are slightly contaminated by granulation velocities in the highest wavenumbers and from the inclusion of the $n = 1$ modes at lower ℓ. The inferred mode energy probability distribution is plotted in Figures 8 a-c for a selection of wavenumbers. Since the energies are uncertain up to a constant multiplicative factor, no scale is given of the energy axis. The exponential distribution with the same observed mean is also plotted. Although the theoretical curve is not a best fit, it conforms well to the data.

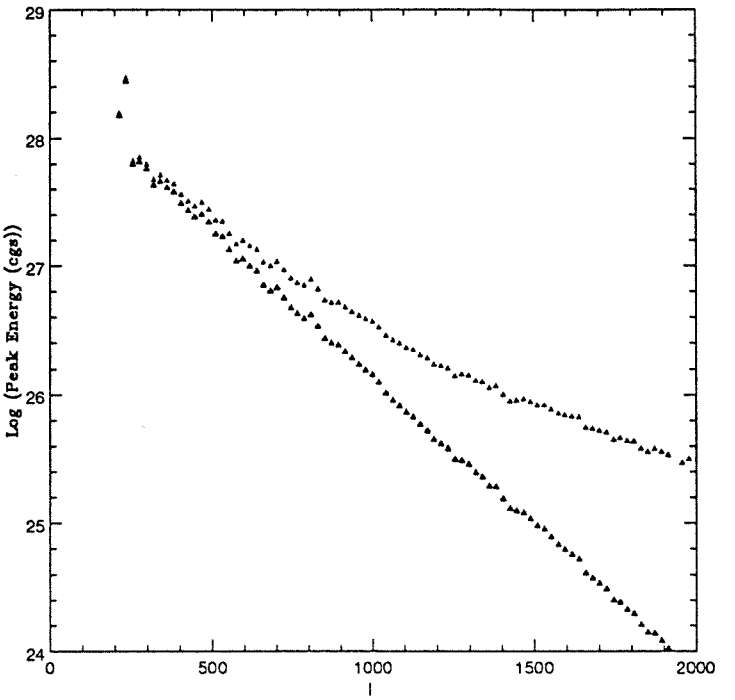

Figure 4.7: Variation of Peak Modal Energy with Wavenumber. The open triangles are the uncorrected data, and dark triangles are for the seeing corrected energies. In both cases, the decrease in mode energy is approximately exponential.

4.4 Discussion

The central result of this analysis is the demonstration of the exponential distribution obeyed by the mode energies. This favors the theory of stochastic excitation, but does not necessarily rule out other proposed mechanisms. For the most part, our mode energies and frequencies are in qualitative agreement with Kaufman (1991), although there remains an unresolved discrepancy concerning the f-mode frequency shift. There is substantial agreement with the energy measurements of Rhodes *et al.* (1991), and departures of order unity in the estimates are accounted for by the crude correction of the MTF to the spectra. We believe the decline in power with decreasing n is real.

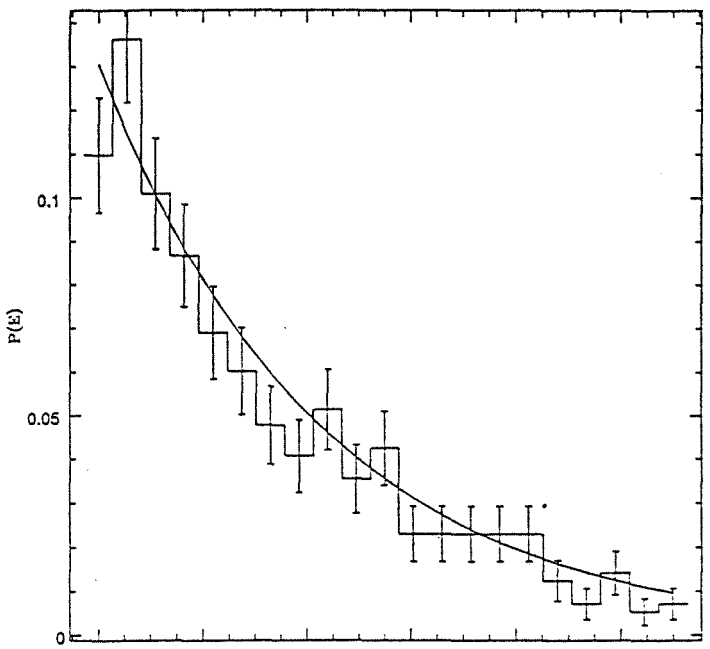

Figure 4.8a: Selected Mode Energy Probability Distribution Function. The sample includes 565 modes $\ell \sim 500$. The error bars cover the range of *a priori* probabilities consistent with the distribution.

Appendix 4.1

Fokker-Planck Equation for Stochastic SHO Excitation

Consider a damped harmonic oscillator with mass, M, frequency, ω_0, and damping constant, Γ. If the oscillator is subject to a time dependent force, the amplitude obeys the equation

$$\ddot{x} + \Gamma\dot{x} + \omega_0^2 x = \frac{F(t)}{M}. \qquad (A4.1.1)$$

Let the driving force, F, be due to white noise

$$\frac{F}{M\omega_0} = \frac{d\xi}{dt}, \qquad (A4.1.2)$$

where ξ is a Wiener Process obeying

$$< d\xi >= 0 \qquad (A4.1.3)$$

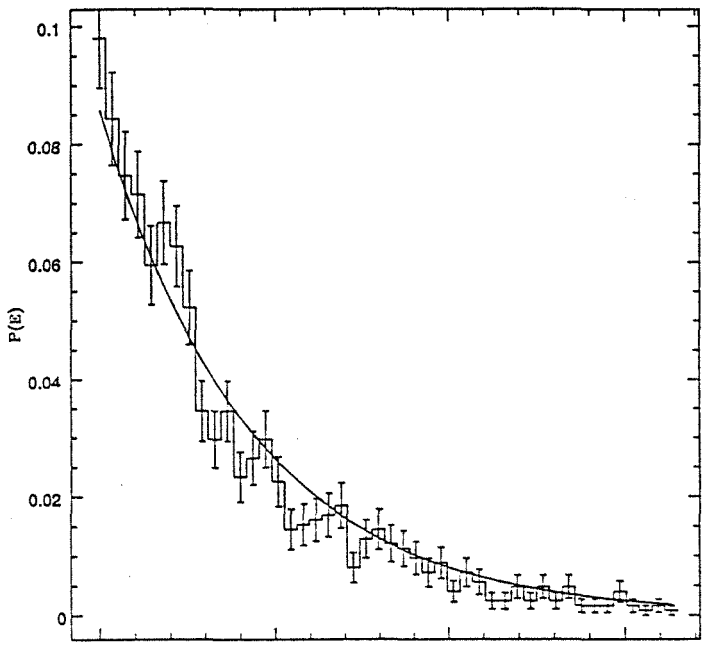

Figure 4.8b: Selected Mode Energy Probability Distribution Function. The sample includes 1245 modes $\ell \sim 1000$. The error bars cover the range of *a priori* probabilities consistent with the distribution.

and

$$< (d\xi)^2 >= \mathcal{D}dt, \qquad (A4.1.4)$$

according to the Ito Calculus (see Karatzas and Shreve (1988)). The constant $\mathcal{D}$ is the *diffusion coefficient* of the process.

Define Coordinates

$$x_1 \equiv x \qquad (A4.1.5)$$

$$x_2 \equiv \dot{x}/\omega_0 \qquad (A4.1.6)$$

and a mode energy

$$E(x_1, x_2) \equiv \frac{M\omega_0^2}{2}(x_1^2 + x_2^2). \qquad (A4.1.7)$$

Then the Fokker-Planck equation for the probability density $p(x_1, x_2, t)$ is given by

$$\frac{1}{\omega_0}\frac{\partial p}{\partial t} + \frac{\partial p}{\partial \phi} = \frac{\partial}{\partial x_2}\left(\alpha x_2 p + \lambda_D^2 \frac{\partial p}{\partial x_2}\right), \qquad (A4.1.8)$$

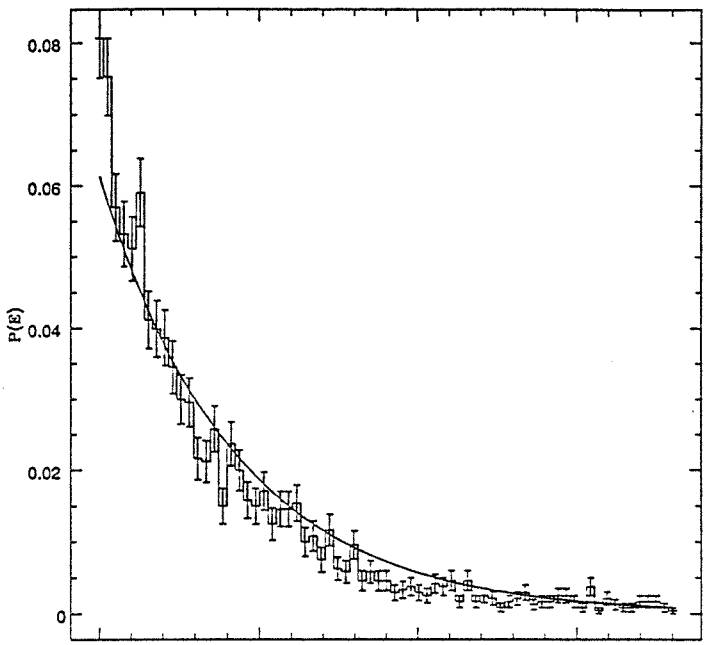

Figure 4.8c: Selected Mode Energy Probability Distribution Function. The sample includes 2405 modes $\ell \sim 2000$. The error bars cover the range of *a priori* probabilities consistent with the distribution.

where

$$\phi \equiv \arctan(x_1/x_2), \tag{A4.1.9}$$

$$\alpha = \Gamma/\omega_0, \tag{A4.1.10}$$

and

$$\lambda_D^2 \equiv \mathcal{D}/2\omega_0. \tag{A4.1.11}$$

The stationary distribution ($\partial p/\partial t = 0$) is given by

$$p(x_1, x_2) = \frac{\Gamma}{\pi\mathcal{D}} \exp\{-\Gamma/\mathcal{D}(x_1^2 + x_2^2)\}, \tag{A4.1.12}$$

and this is the only such solution which is normalizable. Using (A4.1.7), the joint distribution (A4.1.12) corresponds to a mode energy distribution of the Boltzmann type

$$\tilde{p}(E) = \frac{1}{\overline{E}} \exp\{-E/\overline{E}\}, \tag{A4.1.13}$$

where

$$\overline{E} \equiv M\omega_0^2 \mathcal{D}/2\Gamma \qquad (A4.1.14)$$

is the mean energy of the oscillator. This derivation agrees with that of Kumar *et al.* (1988).

For comparison with the solar p- and f-modes, the mass behaves like the mode mass, the frequency like the mode frequency, and Γ is related to the linewidth. Although the simple White Noise model may be hard to justify from first principles, it provides insight into the mode energy distribution. One expects the actual excitation to be broad-banded in frequency.

Chapter 4 References

Cacciani, A., Moretti, P. F., Papaldo, D., and Paverani, E. 1993, *Solar Phys.* **144**, 205.

Christensen-Dalsgaard, J. 1982, solar model.

Dollfus, A. 1990, *Solar Phys.* **129**, 1.

Fernandes, D. N. 1992, *The Detection and Characterization of High Frequency and High Wavenumber Solar Oscillations*, Ph.D. Thesis, Stanford.

Fernandes, D. N., Scherrer, P. H., Tarbell T. D., and Title, A. M. 1992, *Ap. J.* **392**, 736.

Gabriel, M. 1993a, *Astron. Astrophys.* **274**, 931.

Gabriel, M. 1993b, *Astron. Astrophys.* **274**, 935.

Goldreich, P., and Kumar, P. 1990, *Ap. J.* **363**, 694.

Goldreich, P., and Kumar, P. 1991, *Ap. J.* **374**, 366.

Goldreich, P., and Murray, N. 1994, *Ap. J.* **424**, 480.

Goldreich, P., Murray, N., and Kumar, P. 1994, *Ap. J.* **424**, 466.

Karatzas, I., and Shreve, S. 1988, *Brownian Motion and Stochastic Calculus* (Berlin: Springer-Verlag).

Kaufman, J. M. 1991, *Frequencies and Amplitudes of High-Degree Solar Oscillations*, Ph.D. Thesis, Caltech.

Kumar, P. 1988, unpublished programs.

Kumar, P., Franklin, J., and Goldreich, P. 1988, *Ap. J.* **328**, 879.

Libbrecht, K. G., and Kaufman, J. M. 1988, *Ap. J.* **324**, 1172.

Press, W. H., Flannery, B. P., Teukolsky, S. A., and Vetterling, W. T. 1992, *Numerical Recipes: The Art of Scientific Computing* 2nd Ed. (Cambridge: Cambridge University Press).

Rhodes, E. J., Jr., Cacciani, A., and Korzennick, S. G. 1991, *Adv. Space Res.* **11**, 17.

Tarbell, T., Peri, M., Frank Z., Shine, R., and Title, A. 1988, *Observations of F- and P-Mode Oscillations of High Degree* ($500 < l < 2500$) *in Quiet and Active Sun*, in *Seismology of the Sun and Sun-like Stars*, ESA Symposium Proceedings.

Tomczyk, S. 1988, *Measurement of the Rotational Frequency Splitting of the Solar Five-Minute Oscillations* Ph.D. Thesis, UCLA.

CHAPTER 5

Variational Principle for an Incompressible Fluid

The equation of motion for an inviscid, incompressible fluid is derived from a variational principle without using a Lagrange multiplier to impose the constraint of incompressibility. These results may be used to investigate non-linear coupling of incompressible modes.

5.1 Introduction

Variational principles in fluid dynamics have proven useful in solving wave interaction problems (Dewar (1970); Kumar and Goldreich (1989)). The original principle for compressible fluids due to Herivel (1954) has been generalized to magneto-fluids (Katz (1961); Su (1961); Newcomb (1962); Lundgren (1963)). The incompressible case is less tractable, but admits broad application, from the study of water waves in Naval Research to the calculation of three mode coupling among g-modes (Wu *et al.* (1994)). In this chapter, a variational principle for the incompressible fluid is presented for later use in calculations of this type.

The natural manner in which to deal with incompressibility is to include a 'force of constraint' in the action by means of a Lagrange multiplier. While this method works, another approach is available which is more suitable for calculation. The Lagrangian density $\mathcal{L}$ is varied with respect to two fields: one component of the displacement field (ξ_z), and the scalar potential for the solenoidal part of the transverse velocity ($A : \mathbf{v}_{\perp s} = \nabla \times (A\hat{z})$); this field decomposition is permited by the fact that only two components of the

velocity field are independent for an incompressible fluid. Since the pressure does no work on the fluid ($-p\nabla \cdot \mathbf{v} = 0$), it contributes no potential energy to the Lagrangian. In fact, it appears nowhere in our calculation. The 'force of constraint' is manifest in the choice of generalized position variables.

The Lagrangian can be expanded to any order in ξ_z and A. The second order yields a linear wave equation and the three mode coupling is described by the third order. Assuming that $\nabla_\perp \rho_0 = \mathbf{0}$ and $\mathbf{F}_{\text{int}} = -\nabla p$ (i.e., a conservative constraint), we see below that the field A is of order $O(\xi_z^2)$. It does not appear in $\mathcal{L}$ until the fourth order, and hence, does not affect the three mode interactions. Although ξ_z evolves independently of A in the lowest three orders, A may be computed once ξ_z is known to lowest order. Variation of the fourth order $\mathcal{L}$ with respect to A gives the appropriate equation.

In the next section, the variational principle is derived and applied to the problem of gravity waves in a power-law atmosphere. The second and third order contributions to $\mathcal{L}$ are calculated explicitly, using an infinite-dimensional configuration space of the complex wave components $\{\xi_{z\mathbf{k}}\}, \{A_{\mathbf{k}}\}$. Finally, the Hamiltonian is given, along with some technical points in the last section to be understood when applying these results. Appendix 5.1 clarifies the geometric issues in the discussion, and Appendix 5.2 exhibits our Fourier conventions.

5.2 Derivation of the Principle

The equations describing an inviscid fluid are

$$\rho\left(\frac{\partial \mathbf{v}}{\partial t} + \mathbf{v}\cdot\nabla\mathbf{v}\right) = -\nabla p + \mathbf{F}_{\text{ext}} \tag{5.1}$$

$$\frac{\partial \rho}{\partial t} + \mathbf{v}\cdot\nabla\rho = 0 \tag{5.2}$$

and

$$\nabla \cdot \mathbf{v} = 0, \tag{5.3}$$

where $\rho, p, \mathbf{v}$ and $\mathbf{F}_{\text{ext}}$ are the density, pressure, velocity and external force, respectively. We seek a variational principle to describe fluid motions with

respect to a background state of hydrostatic equilibrium ($\mathbf{v}_0 \equiv \mathbf{0}$). To simplify the discussion, we restrict our attention to the case in which the unperturbed density is of the form $\rho_0(z) \propto z^m$, and where the only external force is a constant gravitational field $\mathbf{F}_{\rm ext} = \rho g \hat{z}$.

It is convenient to consider the Lagrangian displacement field defined as

$$\boldsymbol{\xi}(\mathbf{x}, t) = \mathbf{x}'(\mathbf{x}, t) - \mathbf{x}, \tag{5.4}$$

where $\mathbf{x}'$ is the position of the fluid element located at $\mathbf{x}$ in the unperturbed state. The field $\boldsymbol{\xi}$ is related to the velocity through the implicit relation

$$\mathbf{v}'(\mathbf{x}', t) = \mathbf{v}(\mathbf{x} + \boldsymbol{\xi}(\mathbf{x}, t), t) = \frac{\partial \boldsymbol{\xi}}{\partial t}(\mathbf{x}, t), \tag{5.5}$$

and to the density by

$$\rho'(\mathbf{x}', t) = \rho(\mathbf{x} + \boldsymbol{\xi}(\mathbf{x}, t), t) = \rho_0(\mathbf{x}). \tag{5.6}$$

Equation (5.6) is equivalent to the statement of mass conservation (5.2), while (5.5) is a fundamental relation. To express the condition (5.3) in terms of $\boldsymbol{\xi}$, notice that

$$\nabla_{\mathbf{x}'} \cdot \mathbf{v}' = \mathcal{J}_{ij}^{-1} \frac{\partial}{\partial t} \mathcal{J}^{ji} = 0 \tag{5.7}$$

where $\mathcal{J}_{ij} \equiv \partial x_i' / \partial x_j$. One can show that (5.7) is equivalent to

$$\mathcal{J} \equiv \|\mathcal{J}\| = 1 \tag{5.8}$$

where $\mathcal{J}$ is the Jacobian of the coordinate transformation $\mathbf{x}' \rightarrow \mathbf{x}$. (5.8) connects the constraint on $\mathbf{v}$ to one on $\boldsymbol{\xi}$. Notice that $\mathcal{J}$ is cubic in $\boldsymbol{\xi}$ in three dimensions. Kumar and Goldreich (1989) show that $\mathcal{J}$ is given by

$$\mathcal{J} = 1 + \nabla \cdot \boldsymbol{\xi} + \frac{1}{2} \left((\nabla \cdot \boldsymbol{\xi})^2 - \xi_{i,j} \xi^{j,i} \right) + O(\xi^3) \tag{5.9}$$

to second order. In Appendix 5.1, it is shown that $\mathcal{J}$ can be put in the form

$$\mathcal{J} = 1 + \nabla \cdot \mathbf{j}, \tag{5.10}$$

where $\mathbf{j}$ is the vector

$$\mathbf{j} = \boldsymbol{\xi} - \boldsymbol{\xi} \cdot \nabla \boldsymbol{\xi} + \frac{1}{2} \nabla \boldsymbol{\xi} \boldsymbol{\xi} + 0(\xi^3). \tag{5.11}$$

This vector has an interesting geometric interpretation as the *non-linear displacement field.*

If we set the external force to zero, according to Hamilton's Principle, the Lagrangian for the fluid is

$$L = \int d^3\mathbf{x}\mathcal{L} = T = \int d^3\mathbf{x}' \frac{1}{2}\rho' v'^2 = \int d^3\mathbf{x} \frac{1}{2}\rho_0 v'^2 = \int d^3\mathbf{x} \frac{1}{2}\rho_0 \left| \frac{\partial \boldsymbol{\xi}}{\partial t} \right|^2, \tag{5.12}$$

since the only form of energy in the dynamics is kinetic. To vary $\mathcal{L}$ with respect to $\boldsymbol{\xi}$, the condition (5.3) must be imposed through an undetermined Lagrange multiplier such as

$$\tilde{\mathcal{L}} = \mathcal{L} + \lambda(\mathcal{J} - 1). \tag{5.13}$$

To lowest order, (5.1) implies that $\lambda = p$. This approach is problematic since p is a functional of $\boldsymbol{\xi}$; in general, one must solve a partial differential equation to determine the pressure, and eliminate it in favor of the displacement field. Moreover, since only two of these fields are independent (by (5.9)), this Lagrangian is not suitable for expansion in powers of ξ.

An alternative method is to enforce the solenoidal constraint by making the symmetry explicit in the form of $\mathbf{v}$. For example, one might use only two of the displacement field components, and express the kinetic energy associated with the third as an effective potential, as in the case of Kepler's problem. Through an appropriate choice of independent fields, the equation of motion for the waves fields may be derived without requiring a calculation of the pressure. The first obvious choice is to consider the pair of scalar fields σ and τ which are the Euler potentials for the velocity ($\mathbf{v} = \nabla\sigma \times \nabla\tau$). This is commonly done when studying magnetic fields (see Willette (1988) and references therein). Unfortunately, the variation leads to complicated non-linear elliptical partial

differential equations with no direct connection to the equation of motion, and which do not reproduce the linear wave equations in a simple way.

The fact that p must be eliminated from the momentum equation to solve for $\boldsymbol{\xi}$ implies that the form of $\mathcal{L}$ may not be given in terms of simple functions of spatial coordinates. One has to work with the Fourier components of the displacement field to make any progress. For this reason, consider the one-dimensional Lagrangian density

$$\overline{\mathcal{L}} \equiv \int d^2\mathbf{x}_\perp \mathcal{L} = \int d^2\mathbf{x}_\perp \frac{1}{2}\rho_0(z)|\mathbf{v}'|^2. \tag{5.14}$$

Since $\nabla_\perp \rho_0 = \mathbf{0}$, one may make use of Parseval's Theorem to show that

$$\overline{\mathcal{L}} = \sum_{\mathbf{k}} \frac{1}{2}\rho_0(z)\left|\frac{\partial \boldsymbol{\xi}_{\mathbf{k}}}{\partial t}\right|^2, \tag{5.15}$$

where $\boldsymbol{\xi}$ has been expanded in Fourier modes

$$\boldsymbol{\xi}(\mathbf{x}_\perp, z, t) = \sum_{\mathbf{k}} \boldsymbol{\xi}_{\mathbf{k}}(z,t)e^{i\mathbf{k}\cdot\mathbf{x}_\perp}. \tag{5.16}$$

(See Appendix 5.2 for a discussion of our Fourier conventions.) Notice that the reality of $\boldsymbol{\xi}$ implies that $\boldsymbol{\xi}^*_{-\mathbf{k}} = \boldsymbol{\xi}_{\mathbf{k}}$.

The goal of this approach is to enforce the constraint (5.8) explicitly in (5.15) and reduce the problem to two dimensions. Consider decomposing the velocity field into the sum

$$\mathbf{v} = \mathbf{v}_0 + \tilde{\mathbf{v}}, \tag{5.17}$$

where $\mathbf{v}_0$ satisfies

$$\mathbf{v}_{0\perp\mathbf{k}_\perp} = \frac{i\mathbf{k}_\perp}{k_\perp^2}\frac{\partial v_{z\mathbf{k}_\perp}}{\partial z}, \tag{5.18}$$

and $v_{0z} = v_z$. It follows that

$$\nabla \cdot \tilde{\mathbf{v}} = 0 \tag{5.19}$$

and

$$\hat{z} \cdot \tilde{\mathbf{v}} = 0. \tag{5.20}$$

Equations (5.19) and (5.20) can be satisfied only if $\tilde{\mathbf{v}}$ is of the form

$$\tilde{\mathbf{v}} = \nabla \times (\psi \hat{z}) = \nabla\psi \times \hat{z} = \nabla_\perp \times (\psi \hat{z}). \tag{5.21}$$

To make comparison of $\tilde{\mathbf{v}}$ and $\mathbf{v}_0$ convenient, we write $\psi = \partial A/\partial t = \dot{A}$. This decomposition forces $\overline{\mathcal{L}}$ to be a functional of two fields only: v_z and A. Since the modes are expressed in terms of the displacement field, v_z is further expressed as a functional of ξ_z and A, the two fundamental independent fields. It follows from (5.5) that

$$v_z = \frac{\partial \xi_z}{\partial t} - \boldsymbol{\xi} \cdot \nabla \xi_z + O(\xi_z^3). \tag{5.22}$$

In the linear wave equation, the field A does not appear, so clearly $A = O(\xi_z^2)$. This depends on the fact that the constraint force is due to a simple scalar pressure. Hence, to order $O(\xi_z^3)$, the second term on the right-hand side of (5.22) depends only on ξ_z. With these comments in mind, let us now expand $\overline{\mathcal{L}}$ in powers of ξ_z and A and calculate the second and third order Lagrangians. One has that

$$|\mathbf{v}'|^2 = |\mathbf{v}(\mathbf{x} + \boldsymbol{\xi})|^2 \tag{5.23}$$

$$= \left|\frac{\partial \xi_z}{\partial t}\right|^2 + |\mathbf{v}'_{0\perp}|^2 + 2\mathbf{v}'_{0\perp} \cdot \tilde{\mathbf{v}}'_\perp + |\tilde{\mathbf{v}}'_\perp|^2.$$

Consider each term separately. The first one is already in a form suitable for variation, but the others require a bit of work. To expand the second term in $\boldsymbol{\xi}$, notice that

$$\mathbf{v}'_{0\perp} = \mathbf{v}_{0\perp} + \boldsymbol{\xi} \cdot \nabla \mathbf{v}_{0\perp} + O(\xi_z^2) \tag{5.24}$$

The first term in (5.24) gives contributions to all orders above $O(\xi_z)$. To get the lowest two orders, we work in $\mathbf{k}_\perp$ space and find

$$\int d^2\mathbf{x}_\perp |\mathbf{v}'_{0\perp}|^2 = \sum_{\mathbf{k}} |\mathbf{v}'_{0\perp\mathbf{k}}|^2 \tag{5.25}$$

$$= \sum_{\mathbf{k}} \frac{1}{k^2} |\dot{\xi}'_{z\mathbf{k}}|^2 -$$

$$2 \sum_{\substack{\mathbf{k}_1,\mathbf{k}_2,\mathbf{k}_3 \\ \mathbf{k}_1+\mathbf{k}_2+\mathbf{k}_3=0}} \frac{1}{k_3^2} \dot{\xi}'_{z\mathbf{k}_3}$$

$$\left\{ \xi'_{z\mathbf{k}_1} \dot{\xi}'_{z\mathbf{k}_2} + k_1^2 k_2^2 B_{12}^2 \xi'_{z\mathbf{k}_1} \dot{\xi}'_{z\mathbf{k}_2} + k_1^2 B_{12} \xi_{z\mathbf{k}_1} \dot{\xi}''_{z\mathbf{k}_2} + k_2^2 B_{12} \xi''_{z\mathbf{k}_1} \dot{\xi}_{z\mathbf{k}_2} \right\},$$

where

$$B_{12} = B_{21} = \frac{i\mathbf{k}_1 \cdot i\mathbf{k}_2}{k_1^2 k_2^2}, \tag{5.26}$$

and the notation $\cdot \equiv \partial_t$ and $' \equiv \partial_z$ is unambiguous if it is applied only to the fundamental fields ξ_z and A. In deriving (5.25), one makes use of the lowest order behavior of $\boldsymbol{\xi}_\perp$ in its dependence on ξ_z; in doing so, the error introduced is of order $O(\xi_z^4)$. Notice that momentum conservation for the three wave interactions is enforced through the restricted sum

$$\mathbf{k}_1 + \mathbf{k}_2 + \mathbf{k}_3 = 0 \tag{5.27}$$

which will be true of all the contributions to $\overline{\mathcal{L}}_3$, the third order contribution to $\overline{\mathcal{L}}$.

The remaining terms in (5.23) do not contribute until order $O(\xi_z^4, \xi_z^2 A, A^2)$. This is valid for the last one, but somewhat subtle for the penultimate. Up to the fourth order, one has

$$\int d^2\mathbf{x}_\perp \mathbf{v}'_{0\perp} \cdot \tilde{\mathbf{v}}'_\perp = \int d^2\mathbf{x}_\perp (\mathbf{v}_{0\perp} \cdot \tilde{\mathbf{v}}_\perp + O(\xi_z^4, \xi_z^2 A, A^2)) \tag{5.28}$$

$$= \sum_{\substack{\mathbf{k}_1,\mathbf{k}_2 \\ \mathbf{k}_1+\mathbf{k}_2=0}} \hat{z} \cdot \frac{i\mathbf{k}_1 \times i\mathbf{k}_2}{k_1^2} \dot{\xi}'_{z\mathbf{k}_1} \dot{A}_{\mathbf{k}_2} = 0$$

by momentum conservation. The above is true even though $\mathbf{v}_{0\perp} \cdot \tilde{\mathbf{v}}_\perp \neq 0$ pointwise. This shows that the field A does not enter into the dynamics until the fourth order. We have reduced the three mode coupling problem to one involving a single field.

If the fluid is subjected to a constant gravitational field, the *effective* potential

$$\mathcal{V}_g = \frac{1}{2} \frac{d\rho_0}{dz} g \xi_z^2 + \frac{1}{6} \frac{d^2\rho_0}{dz^2} \xi_z^3 + O(\xi_z^4) \tag{5.29}$$

must be subtracted from the above Lagrangian density. Collecting the above results, one has the following lowest order Lagrangians

$$\overline{\mathcal{L}}_2 = \sum_{\mathbf{k}} \frac{1}{2}\rho_0(|\dot{\xi}_{z\mathbf{k}}|^2 + \frac{1}{k^2}|\dot{\xi}'_{z\mathbf{k}}|^2) - \frac{1}{2}\frac{d\rho_0}{dz}g|\xi_{z\mathbf{k}}|^2 \tag{5.30}$$

$$\overline{\mathcal{L}}_3 = -\sum_{\substack{\mathbf{k}_1,\mathbf{k}_2,\mathbf{k}_3 \\ \mathbf{k}_1+\mathbf{k}_2+\mathbf{k}_3=0}} [\frac{1}{6}\frac{d^2\rho_0}{dz^2}\, g\, \xi_{z\mathbf{k}_1}\xi_{z\mathbf{k}_2}\xi_{z\mathbf{k}_3} +$$

$$\frac{\rho}{k_3^2}\dot{\xi}'_{z\mathbf{k}_3}\left\{\xi'_{z\mathbf{k}_1}\dot{\xi}'_{z\mathbf{k}_2} + k_1^2k_2^2B_{12}^2\xi'_{z\mathbf{k}_1}\dot{\xi}'_{z\mathbf{k}_2} + k_1^2B_{12}\xi_{z\mathbf{k}_1}\dot{\xi}''_{z\mathbf{k}_2} + k_2^2B_{12}\xi''_{z\mathbf{k}_1}\dot{\xi}_{z\mathbf{k}_2}\right\}]$$

Due to the $\mathbf{k}$ dependence of the summand, the Fourier expansion does not reduce to a single spatial integral upon inversion.

Variation of $\mathcal{L}_2$ leads to

$$-\frac{\delta\overline{\mathcal{L}}_2}{\delta\xi^*_{z\mathbf{k}}} = \rho_0\frac{\partial^2\xi_{z\mathbf{k}}}{\partial t^2} - \frac{\partial}{\partial z}\left(\frac{\rho_0}{k^2}\frac{\partial^3\xi_{z\mathbf{k}}}{\partial z\partial t^2}\right) + \frac{d\rho_0}{dz}g\xi_{z\mathbf{k}} = 0, \tag{5.31}$$

which is the equation for the linear gravity wave mode $\xi_{z\mathbf{k}}$. The two restoring forces for the oscillator are gravity and the required pressure gradient to keep the motion incompressible. The effective potential for the latter depends on acceleration, so the canonical momentum for this system will differ from the usual case. For the case of a power-law density, equation (5.31) is identical to the wave equation for sound waves in an adiabatically stratified atmosphere with the substitutions

$$Q_{\mathbf{k}} \to \xi_{z\mathbf{k}}, \quad \frac{\omega^2}{gk} \to \frac{gk}{\omega^2} \tag{5.32}$$

(see Appendix 2.3). The boundary condition of vanishing Lagrangian pressure perturbation at the surface $z = 0$ is the same in both cases. The eigenvalues for the mode with n nodes is therefore

$$\omega_{n,k}^2 = \frac{gk}{1 + 2n/m}. \tag{5.33}$$

One can show that the eigenfunctions for the modes form a complete set (see Appendix 2.3). Hence, the component $\xi_{z\mathbf{k}}$ can be expanded as

$$\xi_{z\mathbf{k}} = \sum_{n=0}^{\infty} q_{n,k}(t)\xi_{n,k}(z). \tag{5.34}$$

The three mode coupling can be computed by finding the interaction Hamiltonian $\overline{\mathcal{H}}_3$ and working with action angle variables as in (Kumar and Goldreich (1989)).

Integration by parts cannot eliminate the second spatial derivative of $\xi_{z\mathbf{k}}$ from $\overline{\mathcal{L}}_3$. Hence, a suitable generalized mechanics requires us to view $\overline{\mathcal{L}}_3$ a functional of $\xi_{z\mathbf{k}}$, $\dot{\xi}_{z\mathbf{k}}$, ${\xi_z}'_{\mathbf{k}}$, $\dot{\xi}'_{z\mathbf{k}}$, ${\xi_z}''_{\mathbf{k}}$, and $\dot{\xi}''_{z\mathbf{k}}$. The appropriate functional derivative to put the system in canonical form is

$$\frac{\delta}{\delta\psi} \equiv \sum_{\{n\}} (-1)^n \frac{d^n}{dz^n} \frac{\partial}{\partial \psi^{(n)}}, \tag{5.35}$$

where we notate

$$\psi^{(n)} = \frac{d^n \psi}{dz^n}. \tag{5.36}$$

The canonical momenta are given by

$$\tilde{\pi}_{\mathbf{k}} \equiv \frac{\delta \overline{\mathcal{L}}}{\delta \dot{\xi}_{z\mathbf{k}}}, \tag{5.37}$$

and the equations of motion are

$$\frac{d}{dt} \frac{\delta \overline{\mathcal{L}}}{\delta \dot{\xi}_{z\mathbf{k}}} = \frac{\delta \overline{\mathcal{L}}}{\delta \xi_{z\mathbf{k}}}. \tag{5.38}$$

Defining

$$\pi^{(n)}_{\mathbf{k}} \equiv \frac{\partial \overline{\mathcal{L}}}{\partial \dot{\xi}^{(n)}_{z\mathbf{k}}}, \tag{5.39}$$

the one-dimensional Hamiltonian density is

$$\overline{\mathcal{H}} = \sum_{\{n\}} \sum_{\mathbf{k}} \dot{\xi}^{(n)}_{z\mathbf{k}} \pi^{(n)}_{\mathbf{k}} - \overline{\mathcal{L}}. \tag{5.40}$$

One can show that (5.40) is equivalent to

$$\overline{\mathcal{H}} = \sum_{\mathbf{k}} \dot{\xi}^{(0)}_{z\mathbf{k}} \tilde{\pi}_{\mathbf{k}} - \overline{\mathcal{L}} + \frac{d\Phi}{dz}. \tag{5.41}$$

for some function Φ. This shows that only the $\tilde{\pi}_{\mathbf{k}}$ are meaningful as momenta. As required, the Hamiltonian is a function of the generalized position variables

$\xi_{z\mathbf{k}}^{(n)}$ and the canonical momenta (5.39). Moreover, one can show that $\overline{\mathcal{H}}$ obeys a conservation equation

$$\frac{d\overline{\mathcal{H}}}{dt} = \frac{dF}{dz}, \tag{5.42}$$

for some function F.

5.3 Discussion

A few technical points should be made regarding the above calculation. First, in deriving (5.29), one must notice that the effective force of gravity of the fluid element has three terms to second order

$$\delta\rho g = -\frac{d\rho_0}{dz} g\xi_z - \frac{1}{2}\frac{d^2\rho_0}{dz^2}\xi_z^2 + \nabla\cdot\left(\frac{d\rho_0}{dz} g\xi_z\boldsymbol{\xi}\right) + O(\xi_z^3) \tag{5.43}$$

but the last term does not contribute to $\mathcal{V}_g$. The second order inertia term is

$$-\nabla\cdot\left(\rho_0\frac{\partial^2\boldsymbol{\xi}}{\partial t^2}\boldsymbol{\xi}\right) = \rho\frac{d\mathbf{v}}{dt} - \rho_0\frac{\partial^2\boldsymbol{\xi}}{\partial t^2} + O(\xi^3) \tag{5.44}$$

To this order, it combines with the above term to yield the same equation for δp as in the system without gravity. Since δp is computed by taking $\nabla_\perp\cdot$ of (5.1), gravity does not change the calculation, and the pressure is made an explicit functional of the inertia only. Second, the equation of motion for the $\{A_\mathbf{k}\}$ to lowest order is found by the variation

$$-\frac{\delta\overline{\mathcal{L}}_4}{\delta A_\mathbf{k}^*} = \Big\{\rho_0 k^2\ddot{A}_\mathbf{k} + \tag{5.45}$$

$$\sum_{\substack{\mathbf{k}_1,\mathbf{k}_2\\ \mathbf{k}_1+\mathbf{k}_2=\mathbf{k}}} \hat{z}\cdot\frac{i\mathbf{k}_1\times i\mathbf{k}_2}{k_2^2}\left[\rho_0\xi_{z\mathbf{k}_1}\ddot{\xi}'_{z\mathbf{k}_2} + \rho_0\frac{i\mathbf{k}_1\cdot i\mathbf{k}_2}{k_1^2}\dot{\xi}'_{z\mathbf{k}_1}\dot{\xi}'_{z\mathbf{k}_2} - \frac{d\rho_0}{dz}\xi_{z\mathbf{k}_1}\ddot{\xi}'_{z\mathbf{k}_2}\right]\Big\} = 0$$

Taking $\hat{z}\cdot[\nabla_\perp\times$ of the momentum equation, one finds that (5.45) is indeed valid. To reproduce (5.45), be careful to find all three terms in $\overline{\mathcal{L}}$ which are linear in $A_\mathbf{k}$. Finally, we note that the invariance of $\mathcal{L}$ with respect to the gauge transformation $A \to A + \phi(z,t)$ gives rise to a conserved current, namely $\nabla\cdot\mathbf{v} = 0$. This symmetry principle is a result of Noether's Theorem (see Arnold (1978)).

Appendix 5.1

The Geometry of Incompressibility

THEOREM: The Jacobian of any C^1 coordinate map $\mathbf{x}' : R^N \to M$ can be put in the form

$$\mathcal{J} = \nabla \cdot \mathbf{j}. \tag{A5.1.1}$$

The exterior derivative of the dual to the vector $\mathbf{j}$ ($d^*\mathbf{j}$) is the volume element in the manifold M.

PROOF: Let $\{\partial/\partial x_i\}$ be the Cartesian coordinate basis for R^N. For any C^1 vector field $\mathbf{v}$, the divergence theorem (Schutz (1980)) gives an identity

$$d^*\mathbf{v} = (\nabla \cdot \mathbf{v}) dV_N, \tag{A5.1.2}$$

where dV_N is the volume element in R^N

$$dV_N = dx_1 \wedge \ldots \wedge dx_N. \tag{A5.1.3}$$

Consider the vector $\mathbf{j}$ whose dual is given by

$$^*\mathbf{j} = x_1' dx_2' \wedge \ldots \wedge dx_N'. \tag{A5.1.4}$$

Since $d^*\mathbf{j} = dV_N'$, it follows that $\mathcal{J} = \nabla \cdot \mathbf{j}$. The vector $\mathbf{j}$ is given by

$$j_{i_1} = \epsilon_{i_1 i_2 \ldots i_N} x_1' \frac{\partial x_2'}{\partial x_{i_2}} \cdots \frac{\partial x_N'}{\partial x_{i_N}}, \tag{A5.1.5}$$

where $\epsilon_{\cdot}$ is the N-dimensional permutation operator.

REMARK: In three dimensions, $\mathcal{J}$ is given by

$$\begin{aligned} \mathcal{J} &= \nabla x_1' \cdot (\nabla x_2' \times \nabla x_3') \qquad (A5.1.6) \\ &= \nabla \cdot (x_1' \nabla x_2' \times \nabla x_3'), \end{aligned}$$

which is consistent with (A5.1.5). If one puts

$$\mathbf{x}' = \mathbf{x} + \boldsymbol{\xi}(\mathbf{x}), \tag{A5.1.7}$$

then $\mathbf{j}$ is given by

$$\mathbf{j} = \frac{1}{3}\mathbf{x} + \boldsymbol{\xi} + \frac{1}{2}((\nabla \cdot \boldsymbol{\xi})\boldsymbol{\xi} - \boldsymbol{\xi} \cdot \nabla\boldsymbol{\xi}) \qquad (A5.1.8)$$

$$+\frac{1}{3}(\boldsymbol{\xi} \cdot \nabla\boldsymbol{\xi} - (\nabla \cdot \boldsymbol{\xi})\boldsymbol{\xi}) \cdot \nabla\boldsymbol{\xi} + \frac{1}{6}((\nabla \cdot \boldsymbol{\xi})^2 - \xi_{j,k}\xi^{k,j})\boldsymbol{\xi}.$$

$\mathbf{j}$ is unique up to an antisymmetric derivative just as any exact form may be added to the anti-derivative of dV'_N. $\mathcal{J}$ must be an exact divergence for the Eulerian variation of the non-linear Lagrangian volume variation to vanish for an incompressible fluid

$$\delta\,\Delta V = \delta\,(V' - V) = \delta \int dV(\mathcal{J} - 1) = \int dV \nabla \cdot \delta\mathbf{j} = 0. \qquad (A5.1.9)$$

Finally, notice that the pullback of $\mathbf{j}$ is simply the coordinate in M. For this reason, $\mathbf{j}$ may be called the *non-linear displacement.*

Appendix 5.2

Normalization of Horizontal Transforms

The Fourier mode expansion of a real function F defined over a domain of area L^2 is given by

$$F(\mathbf{x}_\perp) = \frac{1}{L}\sum_{\mathbf{k}} F_{\mathbf{k}} e^{i\mathbf{k}\cdot\mathbf{x}_\perp}. \qquad (A5.2.1)$$

The inversion formula is

$$F_{\mathbf{k}} = \frac{1}{L}\int_{L^2} d^2\mathbf{x}_\perp F(\mathbf{x}_\perp) e^{-i\mathbf{k}\cdot\mathbf{x}_\perp}, \qquad (A5.2.2)$$

which yields Parseval's Theorem in the form

$$\int_{L^2} d^2\mathbf{x}_\perp |F|^2 = \sum_{\substack{\mathbf{k}_1,\mathbf{k}_2 \\ \mathbf{k}_1+\mathbf{k}_2=0}} F_{\mathbf{k}_1} F_{\mathbf{k}_2} = \sum_{\mathbf{k}} |F_{\mathbf{k}}|^2, \qquad (A5.2.3)$$

since the field is real:

$$F_{\mathbf{k}} = F^*_{-\mathbf{k}}. \qquad (A5.2.4)$$

Without loss of generality, the horizontal domain is taken to be a square of area $L^2 = 1$. In the limit $L \to \infty$, the sum $(A5.2.1)$ goes naturally over to a Fourier integral.

Chapter 5 References

Arnold, V. I. 1978 *Mathematical Methods of Classical Mechanics* 2nd Ed. (Berlin: Springer-Verlag).

Dewar, R. L. 1970, *Phys. Fluids* **13**, 2710.

Herivel, J. W. 1954, *Proc. Cambridge Phil. Soc.* **54**, 344.

Katz, S. 1961, *Phys. Fluids* 4, 345.

Kumar, P., and Goldreich, P. 1989, *Ap. J.* **342**, 558.

Lundgren, T. S. 1963, *Phys. Fluids* **6**, 898.

Newcomb, W. A. 1962, *Nucl. Fusion Suppl.* **2**, 451.

Schutz, B. 1980, *Geometrical Methods of Mathematical Physics* (New York: Cambridge University Press).

Su, C. H. 1961, *Phys. Fluids* 4, 1376.

Willette, G. T. 1988, *The Formation of Tangential Discontinuities in Line-Tied Force-Free Fields*, Senior Thesis, Harvard College.

Wu, Y., Goldreich , P., and Willette, G. T. 1994, in preparation.